



HAL
open science

The DEAD box RNA helicase DDX42 is an intrinsic inhibitor of positive-strand RNA viruses

Boris Bonaventure, Antoine Rebendenne, Ana Luiza Chaves Valadão, Mary Arnaud-arnould, Ségolène Gracias, Francisco Garcia de Gracia, Joe Mckellar, Emmanuel Labaronne, Marine Tauziet, Valérie Vivet-boudou, et al.

► To cite this version:

Boris Bonaventure, Antoine Rebendenne, Ana Luiza Chaves Valadão, Mary Arnaud-arnould, Ségolène Gracias, et al.. The DEAD box RNA helicase DDX42 is an intrinsic inhibitor of positive-strand RNA viruses. *EMBO Reports*, 2022, 23 (11), pp.e54061. 10.15252/embr.202154061 . hal-04807258

HAL Id: hal-04807258

<https://hal.science/hal-04807258v1>

Submitted on 27 Nov 2024














HAL is a multi-disciplinary open access archive for the deposit and dissemination of scientific research documents, whether they are published or not. The documents may come from teaching and research institutions in France or abroad, or from public or private research centers.

L'archive ouverte pluridisciplinaire **HAL**, est destinée au dépôt et à la diffusion de documents scientifiques de niveau recherche, publiés ou non, émanant des établissements d'enseignement et de recherche français ou étrangers, des laboratoires publics ou privés.



Distributed under a Creative Commons Attribution - NonCommercial - NoDerivatives 4.0 International License

The DEAD box RNA helicase DDX42 is an intrinsic inhibitor of positive-strand RNA viruses

Boris Bonaventure¹, Antoine Rebendenne¹, Ana Luiza Chaves Valadão¹, Mary Arnaud-Arnould¹ , Ségolène Gracias², Francisco Garcia de Gracia¹, Joe McKellar¹, Emmanuel Labaronne³ , Marine Tauziet¹ , Valérie Vivet-Boudou⁴ , Eric Bernard¹, Laurence Briant¹, Nathalie Gros⁵ , Wassila Djilli¹, Valérie Cournaud⁶, Hugues Parrinello⁷ , Stéphanie Rialle⁷, Mickaël Blaise¹ , Laurent Lacroix⁸ , Marc Lavigne⁹ , Jean-Christophe Paillart⁴ , Emiliano P Ricci³ , Reiner Schulz¹⁰, Nolwenn Jouvenet² , Olivier Moncorgé¹ & Caroline Goujon^{1,*} 

Abstract

Genome-wide screens are powerful approaches to unravel regulators of viral infections. Here, a CRISPR screen identifies the RNA helicase DDX42 as an intrinsic antiviral inhibitor of HIV-1. Depletion of endogenous DDX42 increases HIV-1 DNA accumulation and infection in cell lines and primary cells. DDX42 overexpression inhibits HIV-1 infection, whereas expression of a dominant-negative mutant increases infection. Importantly, DDX42 also restricts LINE-1 retrotransposition and infection with other retroviruses and positive-strand RNA viruses, including CHIKV and SARS-CoV-2. However, DDX42 does not impact the replication of several negative-strand RNA viruses, arguing against an unspecific effect on target cells, which is confirmed by RNA-seq analysis. Proximity ligation assays show DDX42 in the vicinity of viral elements, and cross-linking RNA immunoprecipitation confirms a specific interaction of DDX42 with RNAs from sensitive viruses. Moreover, recombinant DDX42 inhibits HIV-1 reverse transcription *in vitro*. Together, our data strongly suggest a direct mode of action of DDX42 on viral ribonucleoprotein complexes. Our results identify DDX42 as an intrinsic viral inhibitor, opening new perspectives to target the life cycle of numerous RNA viruses.

Keywords DDX42 DEAD-box RNA helicase; intrinsic immunity; RNA viruses; viral inhibition

Subject Categories Immunology; Microbiology, Virology & Host Pathogen Interaction; RNA Biology

DOI 10.15252/embr.202154061 | Received 28 September 2021 | Revised 30 August 2022 | Accepted 7 September 2022 | Published online 26 September 2022

EMBO Reports (2022) 23: e54061

Introduction

The intrinsic and innate immunity are at the frontline against viral invasion and provide a rapid and global defense. The innate immunity relies on viral sensing by pathogen recognition receptors (PRRs) inducing the production of type 1 and 3 interferons (IFNs). Secreted IFNs bind to specific receptors and activate the JAK–STAT signaling cascade, which leads to the expression of hundreds of IFN-stimulated genes (ISGs). The cellular reprogramming induced by ISG expression allows the establishment of an antiviral state that efficiently limits viral replication. Some ISGs are indeed direct antiviral effectors harboring powerful antiviral activities (Schoggins, 2019). Hence, several ISGs, such as the myxovirus resistance protein 1 (MX1) Dynamin Like GTPase, 2',5'-oligoadenylate synthetases (OASs) and ribonuclease L (RNaseL), or protein kinase R (PKR) (Lindenmann, 1962; Zilberstein *et al*, 1978; Zhou, 1993), were identified a long time ago as major players of innate immunity against viruses. More recently, gain-of-function and loss-of-function screens have identified additional IFN-induced antiviral effectors (Schoggins *et al*, 2011; Kane *et al*, 2016; OhAinle *et al*, 2018; Mac Kain *et al*, 2022). A growing list of cellular proteins with various functions has hence been identified as capable of limiting different steps of virus life

- 1 IRIM, CNRS, Université de Montpellier, France
 - 2 Virus Sensing and Signaling Unit, Department of Virology, Institut Pasteur, Université de Paris Cité, CNRS UMR 3569, Paris, France
 - 3 LBMC, Université de Lyon, ENS de Lyon, CNRS, INSERM, Lyon, France
 - 4 Université de Strasbourg, CNRS, Architecture et Réactivité de l'ARN, UPR 9002, Strasbourg, France
 - 5 CEMIPAI, CNRS, Université de Montpellier, Montpellier, France
 - 6 IGMM, CNRS, Université de Montpellier, Montpellier, France
 - 7 Montpellier GenomiX (MGX), Biocampus, CNRS, INSERM, Université de Montpellier, Montpellier, France
 - 8 Institut de Biologie de l'Ecole Normale Supérieure (IBENS), Ecole Normale Supérieure, CNRS, INSERM, Université PSL, Paris, France
 - 9 Department of Virology, Institut Pasteur, Paris, France
 - 10 Department of Medical & Molecular Genetics, King's College London, London, UK
- *Corresponding author. (Lead contact). Tel: +33 4 34 35 94 33; E-mail: caroline.goujon@irim.cnrs.fr

cycles (Doyle *et al*, 2015; Ghimire *et al*, 2018; Chemudupati *et al*, 2019). Viruses have often evolved to counteract the action of these so-called restriction factors (Tenthorey *et al*, 2022). However, type 1 IFNs (e.g. IFN-alpha and -beta) induce, through the expression of ISGs, an antiviral state particularly efficient at inhibiting HIV-1 when cells are pre-exposed to IFN (Doyle *et al*, 2015). The dynamin-like GTPase MX2, and, recently, the restriction factor TRIM5 α , have both been shown to participate in the IFN-induced inhibition of HIV-1 (Kane *et al*, 2013; Goujon *et al*, 2013a; OhAinle *et al*, 2018; Jimenez-Guardeño *et al*, 2019). In addition to the IFN response, antiviral proteins that are constitutively expressed are able to immediately counteract incoming virus replication and are referred to as intrinsic inhibitors; they are part of the so-called intrinsic immunity. While numerous antiviral ISGs have been identified, less is probably known about the extent of the intrinsic, antiviral inhibitor repertoire. The recent identification of TRIM7 as an intrinsic inhibitor of enteroviruses illustrates the fact that important antiviral inhibitors most certainly remain to be revealed (Fan *et al*, 2021).

With the hypothesis that additional HIV-1 inhibitors remained to be identified, we took advantage of the hostile environment induced by IFN to develop a whole-genome, CRISPR/Cas9 screen strategy in order to reveal intrinsic and innate inhibitors. This strategy led us to identify DDX42 as a new intrinsic inhibitor of HIV-1, acting independently of the IFN system. We reveal that endogenous DDX42 is antiviral in various cell types, including primary targets of HIV-1, and impairs the accumulation of viral DNA. Importantly, recombinant DDX42 was able to inhibit HIV-1 reverse transcription *in vitro*. Moreover, our data show a broad activity against lentiviruses and the retrovirus Murine Leukemia Virus (MLV). Reminiscent of other HIV-1 inhibitors such as APOBEC3G, DDX42 also blocks LINE-1 spread by interacting with their RNAs. Interestingly, while three different negative strand RNA viruses were found insensitive to DDX42, several positive strand RNA viruses, including the flavivirus Zika (ZIKV), the alphavirus Chikungunya (CHIKV) and the severe acute respiratory syndrome coronavirus 2 (SARS-CoV-2), were inhibited to various extents by this non-processive RNA helicase. Finally, cross-linking RNA immunoprecipitation assays showed that DDX42 specifically binds to viral RNAs from sensitive viruses, strongly suggesting a direct mode of action. Overall, our study sheds light on a new intrinsic antiviral function of a so far poorly studied DEAD-box RNA helicase, and provide new insights on a broad-spectrum antiviral inhibitor.

Results & Discussion

A genome-wide CRISPR screen identifies DDX42 as an HIV-1 inhibitor

The Genome-Scale CRISPR Knock-Out (GeCKO) sgRNA library (Sanjana *et al*, 2014; Shalem *et al*, 2014, 2015) was used to generate knock-out (KO) populations in the glioblastoma T98G cell line. Despite being an uncommon model for HIV-1 infection, this cell line was chosen because it is highly permissive to HIV-1 infection and potentially able to suppress infection following type 1 IFN pre-treatment (Fig EV1A). Cas9-expressing T98G cells were independently transduced with lentiviral vectors (LVs) coding the two halves of the GeCKO library, at a low multiplicity of infection (MOI)

(Fig 1A). Next-generation sequencing showed more than 94% sgRNA coverage for each sub-library (not shown). Cells were pre-treated with type 1 IFN (IFN-alpha, hereafter called IFN) and incubated with VSV-G-pseudotyped, HIV-1 based LVs coding for an antibiotic resistance cassette. The cells which were successfully infected despite the IFN treatment were selected by survival in the presence of antibiotics. In order to enrich the populations with mutants of interest and to limit the presence of false-positives, two additional rounds of IFN treatment, infection and selection (with different antibiotics) were performed. As expected, the cells enriched after each round became less refractory to HIV-1 infection following IFN treatment (Fig EV1B).

The differential sgRNA abundance between the initial GeCKO populations and selected populations was analyzed by next-generation sequencing (NGS) and the MAGeCK algorithm was used to rank the candidate genes (Fig 1B). An enrichment was observed for 200 genes (RRA score > 0.01), with the best hits being *IFNAR1*, *JAK1* and *STAT2* (Fig 1B). The crucial mediators of type 1 IFN signaling cascade were among the top hits in both screens (with the notable exception of *STAT1*), validating our approach and confirming the identification of relevant genes. Interestingly, most of the other candidates displayed unknown functions, or functions that were *a priori* unrelated to innate immunity. Indeed, we did not identify ISGs known to inhibit HIV-1, such as MX2 (Kane *et al*, 2013; Liu *et al*, 2013; Goujon *et al*, 2013a). Since CRISPR screens are rarely comprehensive (Doench, 2018), we did not expect to identify an exhaustive list of HIV-1 restriction factors. Moreover, apart from genes belonging to the IFN signaling cascade, very little overlap was observed between the two independent screens, performed with two sub-libraries. However, such a poor overlap between biological replicates has been observed before and does not preclude the discovery of valid candidates (Parnas *et al*, 2015; Doench, 2018). The top 25 candidate genes from each screen were selected for further validation. T98G/Cas9 cells expressing HIV-1 CD4 and CXCR4 receptors, as well as Firefly luciferase as an internal control (T98G/Cas9/CD4/CXCR4/Firefly cells), were transduced with sgRNA-expressing LVs to generate individual KO populations, using the identified sgRNA sequences. Four irrelevant, non-targeting sgRNAs, as well as sgRNAs targeting *IFNAR1* and *MX2*, were used to generate negative and positive control populations, respectively. The KO cell populations were pre-treated with IFN and infected with an HIV-1 reporter virus expressing Renilla luciferase and bearing HIV-1 envelope (Goujon *et al*, 2013b; hereafter called HIV-1 Renilla). Infection efficiency was analyzed 30 h later (Fig 1C). As expected (Goujon *et al*, 2013a; Bulli *et al*, 2016; Xu *et al*, 2018), *IFNAR1* and *MX2* KO fully and partially rescued HIV-1 infection from the protective effect of IFN, respectively. The KO of two candidate genes, namely *WARS2* and *DDX42*, allowed a partial rescue of HIV-1 infection from the IFN-induced inhibition, suggesting a potential role of these candidate genes in HIV-1 inhibition.

DDX42 inhibits HIV-1 independently of the interferon response

DDX42 is a member of the DEAD box family of RNA helicases, with RNA chaperone activities (Uhlmann-Schiffler *et al*, 2006) and, as such, retained our attention. Indeed, DEAD box helicases are well-known to regulate HIV-1 life cycle (Taschuk & Cherry, 2020; Bonaventure & Goujon, 2022). However, to our knowledge, the impact

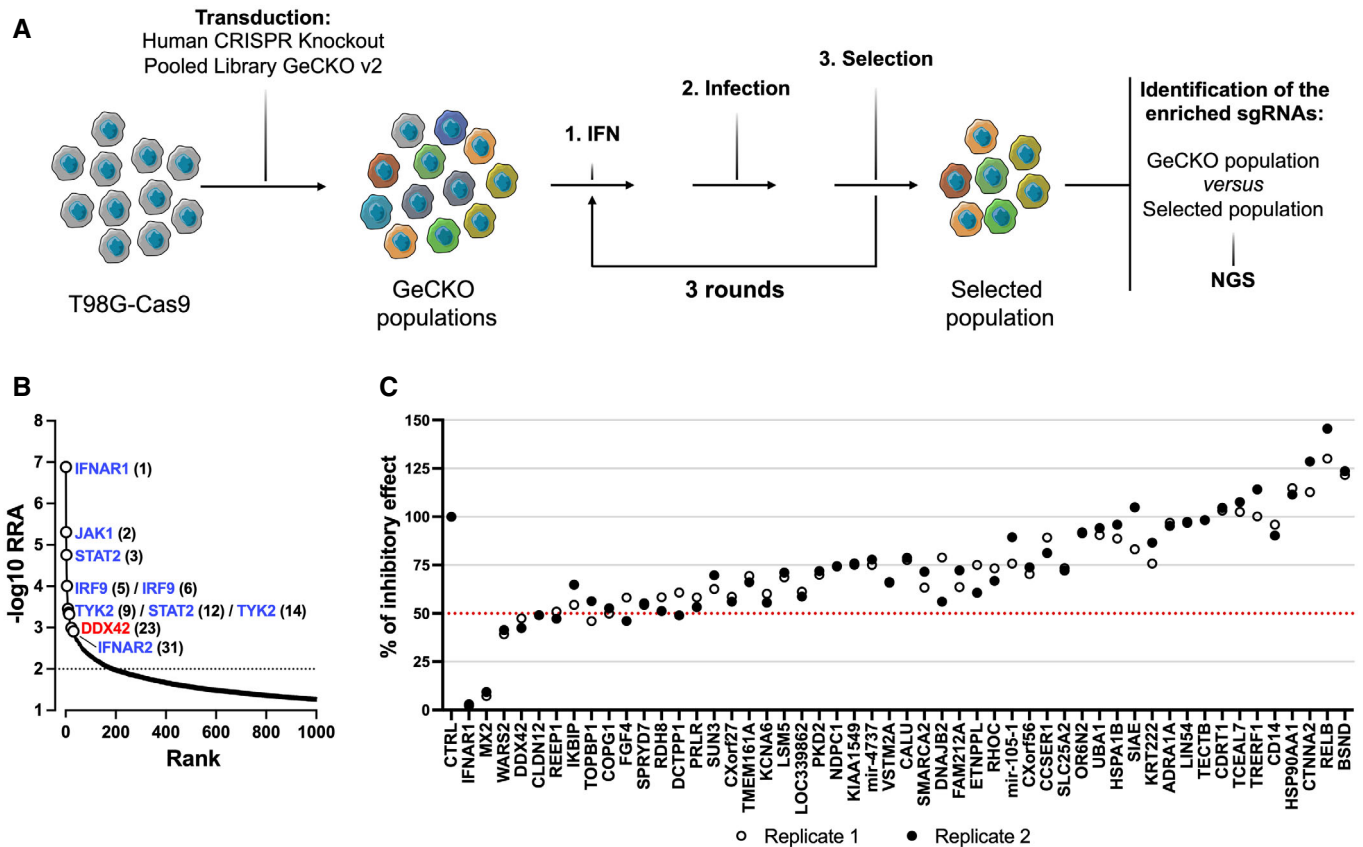


Figure 1. A whole-genome CRISPR/Cas9 screen to identify new HIV-1 inhibitors.

- A** Screen strategy. GeCKO cell populations (obtained by transduction of T98G/Cas9 cells with GeCKO v2 LV library) were IFN-treated, challenged with HIV-1 LVs coding for an antibiotic resistance gene and selected. Three rounds of IFN treatment, infection and selection were performed. Genomic DNAs of initial GeCKO and 3-time selected populations were extracted, the sgRNA-coding sequences amplified and sequenced.
- B** Candidate gene identification. MAGeCK computational statistical tool (Li *et al*, 2014) was used to establish a Robust Rank Aggregation (RRA) score for each gene based on sgRNA enrichment and number of sgRNAs per gene. Genes belonging to the type 1 IFN response pathway (in blue) and DDX42 (in red) are shown (respective ranks into brackets) for 2 independent screens (the results of which were merged in the analysis). The dashed line indicates the significance threshold.
- C** Candidate validation. T98G/Cas9/CD4/CXCR4/Firefly KO populations were generated for the 25 top hits of each screen. The control (CTRL) condition represents the mean of 4 negative CTRL populations, obtained with 4 non-targeting sgRNAs; *IFNAR1* and *MX2* KO populations were used as positive controls. KO cell populations were treated with IFN and infected with HIV-1 Renilla (NL4-3/Nef-IRES-Renilla) and luciferase signals were measured 30 h later (Renilla signals were normalized to Firefly). IFN inhibition (i.e. ratio of untreated / IFN-treated conditions) was calculated and set at 100% inhibition for CTRL. Data from technical duplicates are shown.

of *DDX42* on HIV-1 replication had never been studied. In order to validate the effect of *DDX42* KO on HIV-1 infection in another model cell line, two additional sgRNAs were designed (sgDDX42-2 and -3) and used in parallel to the one identified in the GeCKO screen (sgDDX42-1; Fig 2A). U87-MG/CD4/CXCR4 cells were used here, as we previously extensively characterized the IFN phenotype against HIV-1 in these cells (Goujon *et al*, 2013a, 2013b). Control and *DDX42* KO cell populations were generated and pre-treated or not with IFN prior to infection with HIV-1 Renilla. Of note, CRISPR/Cas9 KO of *DDX42* induced only a partial decrease in *DDX42* protein levels (Fig 2A) and cell populations tended to derive (not shown), suggesting a potential impact of *DDX42* on cell proliferation or long-term survival. We observed however that *DDX42* partial depletion with all 3 sgRNAs significantly improved HIV-1 infection, confirming that endogenous *DDX42* had a negative impact on HIV-1 replication. Interestingly, the increase in infection efficiency induced by *DDX42* KO was observed independently of the IFN treatment. *DDX42* is not an ISG, as shown in several cell lines (U87-MG, T98G,

HEK293T, Jurkat) and in primary T cells and monocyte-derived macrophages (Fig EV1C and GSE46599; Goujon *et al*, 2013a). The fact that the IFN-induced state is at least partially saturable (Fig EV1A) explains why an intrinsic inhibitor of HIV-1, which is not regulated by IFN, could be identified by our approach. Indeed, removing one barrier to infection presumably rendered the cells more permissive and, in this context, IFN had less of an impact on viral replication.

In order to confirm *DDX42*'s effect on HIV-1 infection with an independent approach, we used three different siRNAs to knock-down *DDX42* expression. *DDX42* depletion increased HIV-1 Renilla infection efficiency by 3 to 8-fold in U87-MG/CD4/CXCR4 cells, irrespectively of the presence of IFN (Fig 2B). Of note, *DDX42* depletion was highly efficient (~90% efficiency both at the mRNA and protein levels, Fig 2C) but did not impact cell growth (not shown) nor cell viability over the course of the experiments (Fig EV2A). Wild-type HIV-1 infection was also significantly increased by *DDX42* silencing, as assessed by viral RNA yield (Fig EV2B), by Capsid (CA

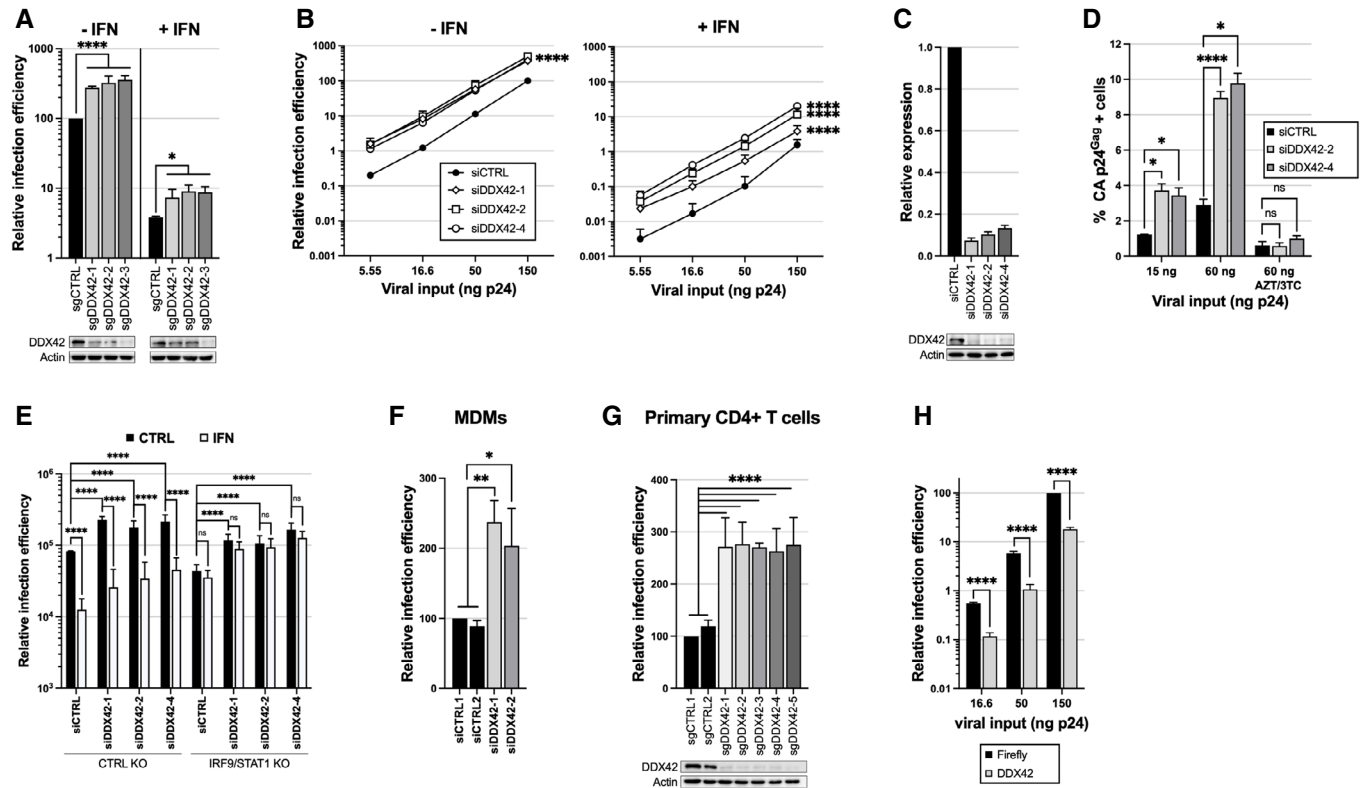


Figure 2. DDX42 is an intrinsic inhibitor of HIV-1.

- A Top: DDX42 KO and CTRL KO U87-MG/CD4/CXCR4/Cas9/Firefly cells were generated using 3 sgRNAs and 4 non-targeting sgRNAs, respectively (for CTRL, the average of data obtained with 4 cell populations is shown). Cells were treated or not with IFN 24 h prior to infection with HIV-1 Renilla (NL4-3/Nef-IRES-Renilla). Relative luminescence results for IFN-treated and -untreated conditions are shown. Two-way ANOVA on log-transformed data with Sidak's test. Bottom: Immunoblot analysis of DDX42 levels is shown for 1 CTRL and DDX42-depleted populations; Actin served as a loading control.
- B siRNA-transfected U87-MG/CD4/CXCR4 cells were treated or not with IFN for 24 h prior to infection with HIV-1 Renilla. Relative luminescence results for IFN-treated and -untreated conditions are shown. Multiple linear regression analysis.
- C DDX42 silencing efficiency measured by RT-qPCR (top) and immunoblot (bottom) in parallel samples from B.
- D DDX42-depleted cells were infected with HIV-1 (WT NL4-3), and infection efficiency was measured by CA p24^{Gag} intracellular staining and flow cytometry analysis. When indicated, cells were treated with azidothymidine (AZT) and lamivudine (3TC). Two-way ANOVA on log-transformed data with Dunnett's test.
- E CTRL and IRF9/STAT1 KO cells were pre-treated or not with IFN for 24 h and infected with HIV-1 Renilla (NL4-3/Nef-IRES-Renilla). Infection efficiency was assessed 24 h later by measuring Renilla activity. Two-way ANOVA on log-transformed data with Dunnett's test.
- F siRNA-transfected MDMs were infected with a CCR5-tropic version of HIV-1 Renilla (NL4-3/R5/Nef-IRES-Renilla). Relative luminescence results from biological triplicates performed with cells from different donors are shown. Two-way ANOVA on log-transformed data with Dunnett's test.
- G Primary CD4⁺ T cells were electroporated with Cas9-sgRNA RNPs using 2 non-targeting sgRNAs (sgCTRL1 and 2) and 5 sgRNAs targeting DDX42. Top: Cells were then infected with HIV-1 Renilla (NL4-3/Nef-IRES-Renilla) and relative infection efficiencies obtained with cells from 3 donors are shown. Two-way ANOVA on log-transformed data with Dunnett's test. Bottom: DDX42 protein levels were determined by immunoblot, Actin served as a loading control. A representative immunoblot is shown.
- H Firefly- or DDX42-expressing U87-MG/CD4/CXCR4 cells were infected with HIV-1 Renilla (NL4-3/Nef-IRES-Renilla). Relative infection efficiencies are shown. Multiple linear regression analysis.

Data information: (A–D) and (F–H), Data represent the mean \pm S.E.M of 3 biological replicates, (E) Data represent the mean \pm S.E.M of 4 biological replicates. *P* values are denoted as follow: ns, not significant, **P* < 0.05, ***P* < 0.01, *****P* < 0.0001. Source data are available online for this figure.

p24^{Gag} intracellular staining in U87-MG/CD4/CXCR4 cells (Fig 2D) and by CA p24^{Gag} production in the supernatant (Fig EV2C). As shown in Fig 2A and B, DDX42's antiviral activity did not require an IFN pre-treatment of the cells. However, one could envisage that DDX42 regulated the IFN responses to HIV-1 infection and thus indirectly favored infection. Therefore, we first checked the induction of 3 prototype ISGs (OAS1, ISG15 and MX1), in the context of DDX42 depletion, HIV-1 infection and/or IFN treatment in U87-MG/CD4/CXCR4 cells (Fig EV2D). We observed that HIV-1 did not induce ISG

expression in these cells (regardless the absence or presence of DDX42), and that DDX42 had no substantial impact on the cell ability to respond to IFN (Fig EV2D). Next, to further exclude a role of IFN signaling in DDX42's antiviral activity, we engineered IRF9/STAT1 double KO U87-MG/CD4/CXCR4 cells, in parallel to control cells. These cells were severely impacted in their ability to respond to IFN as they failed to induce the expression of two prototype ISGs, *IFITM3* and *MX2* (Fig EV2E) and remained permissive to HIV-1 infection following IFN treatment, contrary to the control KO cells

(Fig 2E). Importantly, depletion of DDX42 in IRF9/STAT1 double KO and CTRL cells had a similar, positive impact on HIV-1 infection (Fig 2E), arguing against a role of IFN signaling and ISGs in DDX42's antiviral activity.

We then investigated the impact of DDX42 in HIV-1 primary target cells. In monocyte-derived macrophages (MDMs), we observed that HIV-1 infection was increased by about 2-fold following DDX42 silencing (Fig 2F), whereas DDX42 mRNA abundance was decreased by only 40% (Fig EV2F). Electroporation of pre-assembled Cas9-sgRNA ribonucleoprotein complexes (RNPs) was used to efficiently deplete DDX42 in primary CD4⁺ T cells (Fig 2G). DDX42 depletion increased HIV-1 infection by 2- to 3-fold (Fig 2G), showing a physiological role of DDX42 as an intrinsic inhibitor of HIV-1 in primary CD4⁺ T cells.

Next, in addition to silencing/knockout assays, we analyzed the consequences of DDX42 overexpression on HIV-1 infection. An irrelevant control (Firefly) or DDX42 were ectopically expressed in U87-MG/CD4/CXCR4 and the cells were challenged with HIV-1 (Fig 2H). DDX42 overexpression induced a substantial inhibition of HIV-1 infection (~ 5-fold decrease in infection efficiency in comparison to the control). Interestingly, the expression of K303E DDX42 mutant, which is unable to hydrolyze ATP and is believed to act as a dominant negative (Rocak, 2005; Granneman *et al.*, 2006), increased HIV-1 infection by 3-fold (Fig EV2G), reminiscent of the impact of DDX42 depletion. Altogether, these data showed that endogenous DDX42 is able to intrinsically inhibit HIV-1 infection.

DDX42 inhibits HIV-1 DNA accumulation in cells and *in vitro*

In order to determine which step of HIV-1 life cycle was affected by DDX42, we quantified HIV-1 DNA accumulation over time in DDX42-silenced and control U87-MG/CD4/CXCR4 cells (Fig 3A;

silencing efficiency is shown in Fig 3B). DDX42 depletion increased the accumulation of early and late reverse transcript products (by 2.5- to 8-fold), as well as proviral DNA and 2-long terminal repeat (2-LTR) circles at 48 h post-infection (by 2.5- to 4.5-fold). Importantly, DDX42 silencing did not impact HIV-1 entry, as assessed by a BlaM-Vpr assay (Fig EV3A). These data suggested that endogenous DDX42 could inhibit reverse transcription and/or impact genome stability, leading to a decrease in viral DNA accumulation. Interestingly, recombinant DDX42 (Fig EV3B) was able to efficiently inhibit HIV-1 reverse transcription in an *in vitro* assay. Indeed, we observed a potent and dose-dependent decrease of the minus strand strong-stop DNA synthesis in the presence of DDX42 (13-fold decrease at 2 μ M, 60 min; Fig 3C and D). The amount of the +5 extension product was also significantly reduced (Fig EV3C and D). This clearly showed that DDX42 had the intrinsic ability to decrease reverse transcription in a minimal system. Therefore, we hypothesized that if DDX42 was able to inhibit reverse transcription in a direct manner in cells, it should be found in close proximity to HIV-1 reverse transcription complexes during infection. In agreement with this, proximity ligation assay (PLA) performed on HIV-1 infected MDMs showed that DDX42 was indeed in close vicinity of Capsid (Fig 3E).

DDX42 depletion increases retrovirus infection

We next examined the ability of DDX42 to inhibit infection by various primate lentiviruses, including lab-adapted strains of HIV-1 (NL4-3, IIB), transmitted/founder strains (CH077.t, CH106.c, REJO.c) (Ochsensbauer *et al.*, 2012), HIV-2 and simian immunodeficiency virus from rhesus macaque (SIV_{MAC}). DDX42 was depleted or not in TZM-bl reporter cells prior to infection with VSV-G-pseudotyped lentiviruses, and infection efficiency was monitored

Figure 3. Characterization of DDX42 inhibitory activity against retroviruses and retroelements.

- A siRNA-transfected U87-MG/CD4/CXCR4 cells were infected with WT HIV-1 (NL4-3) and relative amounts of Minus Strand Strong Stop (MSSS), 1st and 2nd Strand Transfer DNAs, and nuclear forms of HIV-1 DNA (proviral DNA, and 2-LTR circles) were quantified by qPCR. DNAs from cells infected for 48 h in the presence of AZT and 3TC were used as a control. Mixed-effects analysis on log-transformed data with Dunnett's test.
- B Silencing efficiency in parallel samples from A.
- C Heat-annealed ODN/RNA 1–294 complex was incubated with HIV-1 RT and increasing concentrations of recombinant DDX42. Reverse transcription was initiated by addition of the four dNTPs. Extension was for 1, 5, 20 or 60 min and samples were analyzed by PAGE 8% (P/T: primer/template; SSDNA: Strong-Stop DNA). A representative autoradiograph is shown.
- D Quantification of 3 biological replicates performed as in C. Two-way ANOVA on log-transformed data with Dunnett's test.
- E PLAs were performed in MDMs infected with HIV-1 or not (N.I. CTRL), using anti-Capsid and anti-DDX42 antibodies (nuclei stained with Hoechst). Images were acquired using a LSM880 Airyscan microscope. Left: representative images, scale-bar: 10 μ m. Right: Average punctae quantified per cell in 3 biological replicates done on MDMs from different donors with mean \pm SD ($n > 65$ cells per condition). Mann-Whitney test.
- F siRNA-transfected TZM-bl cells were infected with the indicated VSV-G-pseudotyped, replication competent viruses and β -galactosidase signals measured 24 h later. Two-way ANOVA on log-transformed data with Dunnett's test.
- G Silencing efficiency in parallel samples from (F).
- H siRNA-transfected U87-MG/CD4/CXCR4 cells were infected with HIV-1- HIV-2- FIV- EIAV-based, GFP-coding LVs and infection efficiency was scored 24 h later by measuring the percentage of GFP expressing cells by flow cytometry. Two-way ANOVA on log-transformed data with Dunnett's test.
- I siRNA-transfected U87-MG/CD4/CXCR4 cells were infected with GFP-coding B-MLV retroviral vector and infection efficiency measured 24 h later by flow cytometry. Simple linear regression analysis.
- J HEK293T were co-transfected with GFP-coding LINE-1 plasmids (RPS-GFP or LRE3-GFP) or with an inactive LINE-1 plasmid (JM111) together with either a Firefly- or DDX42-coding plasmid. GFP expression was measured by flow cytometry 7 days later. Two-way ANOVA on log-transformed data with Sidak's test.
- K HEK293T were co-transfected with pRPS-GFP and a Flag-Firefly- (negative control) or Flag-DDX42-coding plasmid, followed by Flag immunoprecipitation and immunoblot analysis. A representative immunoblot is shown.
- L Left, RNA extraction and LINE-1 RT-qPCR on parallel samples from (K). Two-way ANOVA on log-transformed data with Sidak's test. Right, Percentage of immunoprecipitated RNA. T-test on log-transformed data.

Data information: (A, B) and (D–J), Data represent the mean \pm S.E.M of 3 biological replicates, (L), Data represent the mean \pm S.E.M of 5 biological replicates. P values are denoted as follow: ns, not significant, * $p < 0.05$, ** $p < 0.01$, *** $p < 0.001$, **** $p < 0.0001$.

Source data are available online for this figure.

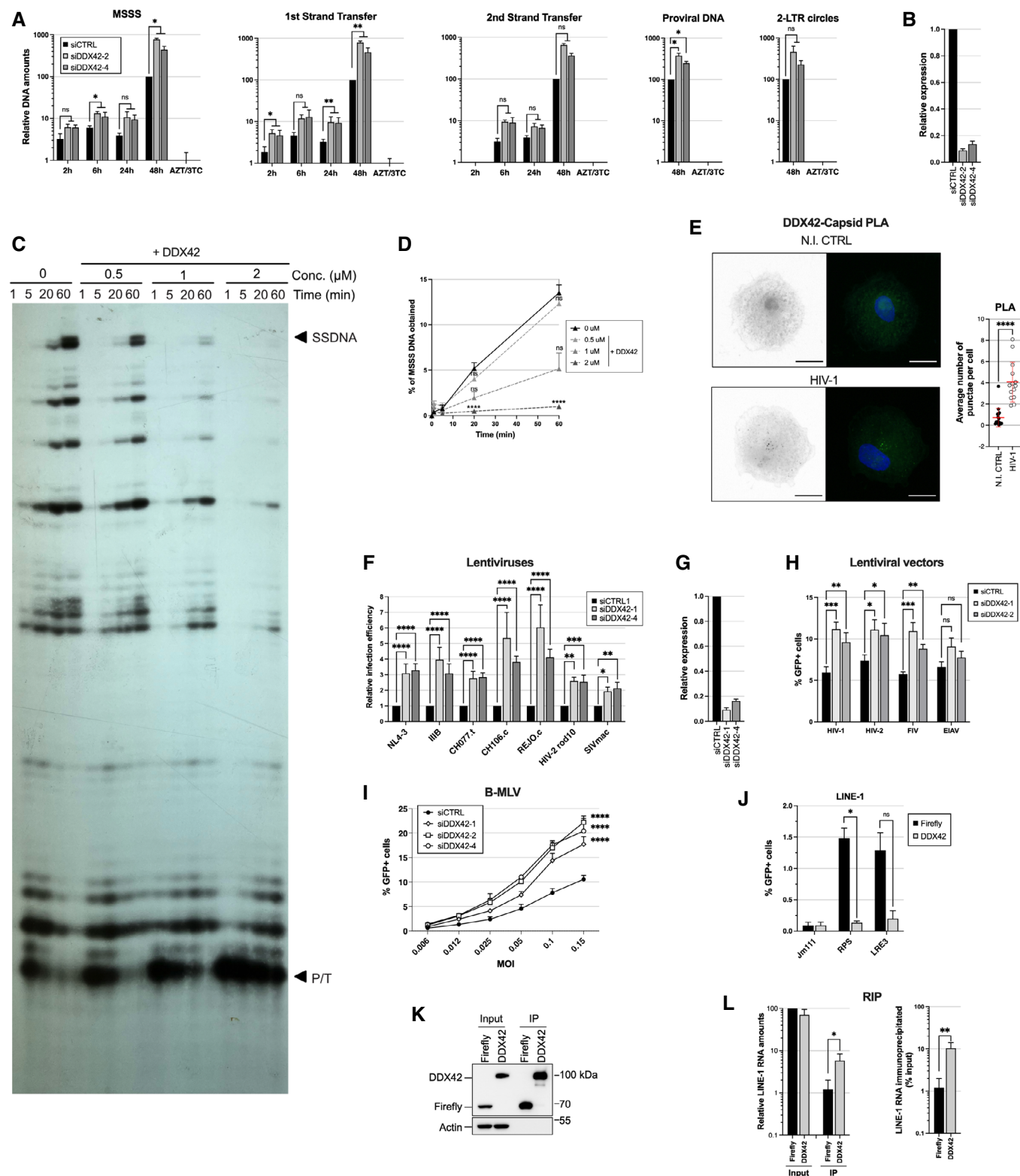


Figure 3.

24 h later (Fig 3F; silencing efficiency is shown in Fig 3G). DDX42 depletion increased infection levels similarly with all the tested strains of HIV-1 (i.e. 3- to 5-fold). HIV-2rod10 and SIV_{MAC} infection

efficiencies were also slightly improved in the absence of DDX42 (~2-fold). The analysis was then extended to two non-primate lentiviruses, equine infectious anemia virus (EIAV) and feline

immunodeficiency virus (FIV), using GFP-coding LVs in U87-MG cells (Fig 3H). DDX42 depletion appeared to increase HIV-1, HIV-2 and FIV LV infection to a similar extent (~2-fold), whereas EIAV infection was less impacted. Of note, DDX42 antiviral activity appeared less potent on HIV-1 LVs compared with full-length HIV-1, which might suggest that genome length or cis-acting elements could play a role in DDX42 inhibition. We also observed that DDX42 depletion led to a significant increase in infection with GFP-coding, MLV-derived vectors (Fig 3I). These results strongly support a general antiviral activity of DDX42 against retroviruses.

DDX42 binds LINE-1 RNAs and inhibits retrotransposition

As previously described in various cell lines including HT1080 cells (Uhlmann-Schiffler *et al*, 2009; Zyner *et al*, 2019), DDX42 could be found in the cytoplasm but is predominantly located in the nuclei of monocyte-derived macrophages (Fig EV3E). Considering that DDX42 showed a broad activity against retroviruses (Fig 3F–I) and seemed to act at the level of reverse transcription (Fig 3A), we investigated whether DDX42 could inhibit retrotransposition. Long interspersed nuclear elements (LINE)-1 are non-LTR retrotransposons, which have been found to be active in the germ line and some somatic cells (Faulkner & Billon, 2018). Interestingly, DDX42 was identified among the suppressors of LINE-1 retrotransposition through a genome-wide screen in K562 cells, although not further characterized (Liu *et al*, 2018). To confirm that DDX42 could inhibit LINE-1 retrotransposition, HEK293T cells were co-transfected with GFP-expressing LINE-1 plasmids (RPS or LRE3) or an inactive LINE-1 (JM111) together with a DDX42- or a control (Firefly)-expressing plasmid (Moran *et al*, 1996). LINE-1 retrotransposition was quantified by flow cytometry 7 days later (Fig 3J). As the GFP cassette is cloned in antisense and disrupted by an intron, GFP is only expressed after LINE-1 transcription, splicing, Orf2p-mediated reverse transcription, and integration (Moran *et al*, 1996). Successful retrotransposition events were observed in > 1.25% of control cells, but in only < 0.25% of DDX42-expressing cells (i.e. a

percentage similar to what observed with the non-active LINE-1), showing that DDX42 ectopic expression suppressed LINE-1 retrotransposition. Next, we investigated whether DDX42 could physically interact with LINE-1 RNAs by performing cross-linking RNA immunoprecipitation. Cells were co-transfected with GFP-expressing LINE-1 RPS plasmid and either flag-tagged-Firefly or -DDX42. Four days later, the cells were treated with formaldehyde, lysed and the flagged proteins immunoprecipitated. The immunoprecipitation eluates were then divided in two; the immunoprecipitated proteins were analyzed by immunoblot (Fig 3K) and their associated RNAs were extracted and quantified by RT-qPCR using LINE-1 specific primers (Fig 3L). A significant enrichment of LINE-1 RNAs was observed with DDX42 immunoprecipitation when compared with the Firefly negative control, showing that DDX42 interacted with LINE-1 RNAs.

DDX42 inhibits various positive-strand RNA viruses

Next, we sought to determine whether DDX42's inhibitory activity was specific towards retroviruses and retroelements, or could be extended to other viruses, as observed for many other anti-HIV-1 proteins, such as ZAP or BST-2/Tetherin (Chemudupati *et al*, 2019; Schoggins, 2019). To this aim, we tested the impact of DDX42 depletion on 10 RNA viruses from six different families: the orthomyxovirus influenza A virus (IAV), the rhabdovirus vesicular stomatitis virus (VSV), the paramyxovirus measles virus (MV), the flaviviruses ZIKV, Japanese encephalitis virus (JEV), Dengue virus serotype 2 (DENV-2) and yellow fever virus (YFV), the alphavirus CHIKV, the coronavirus SARS-CoV-2, which is responsible for the current coronavirus disease (COVID)-19 pandemic, and the seasonal human coronavirus HCoV-229E (Figs 4 and EV4). Strikingly, DDX42 depletion had no significant, positive effect on IAV and VSV in U87-MG cells (Fig 4A and B) or on MV replication in Huh-7 cells (Fig 4C) (silencing efficiency is shown in Fig EV4A). This strongly suggested that manipulating DDX42 expression did not have a broad and unspecific impact on target cells. Interestingly, depletion of endogenous

Figure 4. DDX42 exerts a broad antiviral activity on positive strand RNA viruses and interacts with viral RNAs from targeted viruses.

- A Relative IAV-Nanoluciferase (IAV-NLuc) infection efficiency in siRNA-transfected U87-MG cells (Nanoluciferase activity 16 h post infection). Multiple linear regression analysis.
- B Relative VSV-Firefly infection efficiency in siRNA-transfected U87-MG cells (Firefly activity 24 h post infection). Multiple linear regression analysis.
- C Relative MV-GFP infection efficiency in siRNA-transfected Huh-7 cells (GFP+ cells scored 24 h post infection). Multiple linear regression analysis.
- D Relative ZIKV-Nanoluciferase infection efficiency in siRNA-transfected U87-MG cells (Nanoluciferase activity 24 h post infection). Multiple linear regression analysis.
- E Relative CHIKV-Nanoluciferase infection efficiency in siRNA-transfected U87-MG cells (Nanoluciferase activity 24 h post infection). Multiple linear regression analysis.
- F WT CHIKV infection efficiency in control (–) and IFN-treated (+), siRNA-transfected U87-MG cells analyzed by RT-qPCR on genomic RNA. Two-way ANOVA on log-transformed data with Dunnett's test.
- G Viral production in cell supernatants from U87-MG cells with WT CHIKV (24 h post-infection, MOI 1) measured by plaque assays. Two-way ANOVA on log-transformed data with Dunnett's test.
- H CTRL and IRF9/STAT1 KO U87-MG/CD4/CXCR4 cells were pre-treated or not with IFN for 24 h and infected with CHIKV-NLuc. Infection efficiency was assessed 24 h later by measuring Nanoluciferase activity. Two-way ANOVA on log-transformed data with Dunnett's test.
- I Relative WT SARS-CoV-2 infection in siRNA-transfected A549-ACE2 cells (RdRp RT-qPCR 48 h post-infection). Mixed-effects analysis on log-transformed data with Dunnett's test.
- J Viral production in A549-ACE2 cell supernatants from I (48 h post-infection, MOI 0.05) measured by plaque assays. Two-way ANOVA on log-transformed data with Dunnett's test.
- K Relative HCoV-229E-Renilla infection efficiency in siRNA-transfected Huh7.5.1 cells (Renilla activity 24 h post infection). Two-way ANOVA on log-transformed data with Dunnett's test.
- L CTRL and IRF9/STAT1 KO A549-ACE2 cells were pre-treated or not with IFN for 24 h and infected with SARS-CoV-2-Nanoluciferase. Infection efficiency was assessed 24 h later by measuring Nanoluciferase activity. Two-way ANOVA on log-transformed data with Dunnett's test.

Data information: Data represent the mean \pm S.E.M. of 3 biological replicates (A–E, F for MOI 0.5, and K) or 4 biological replicates (F for MOI 0.1, G–J and L). *P* values are denoted as follow: ns, not significant, **P* < 0.05, ***P* < 0.01, ****P* < 0.001, *****P* < 0.0001.

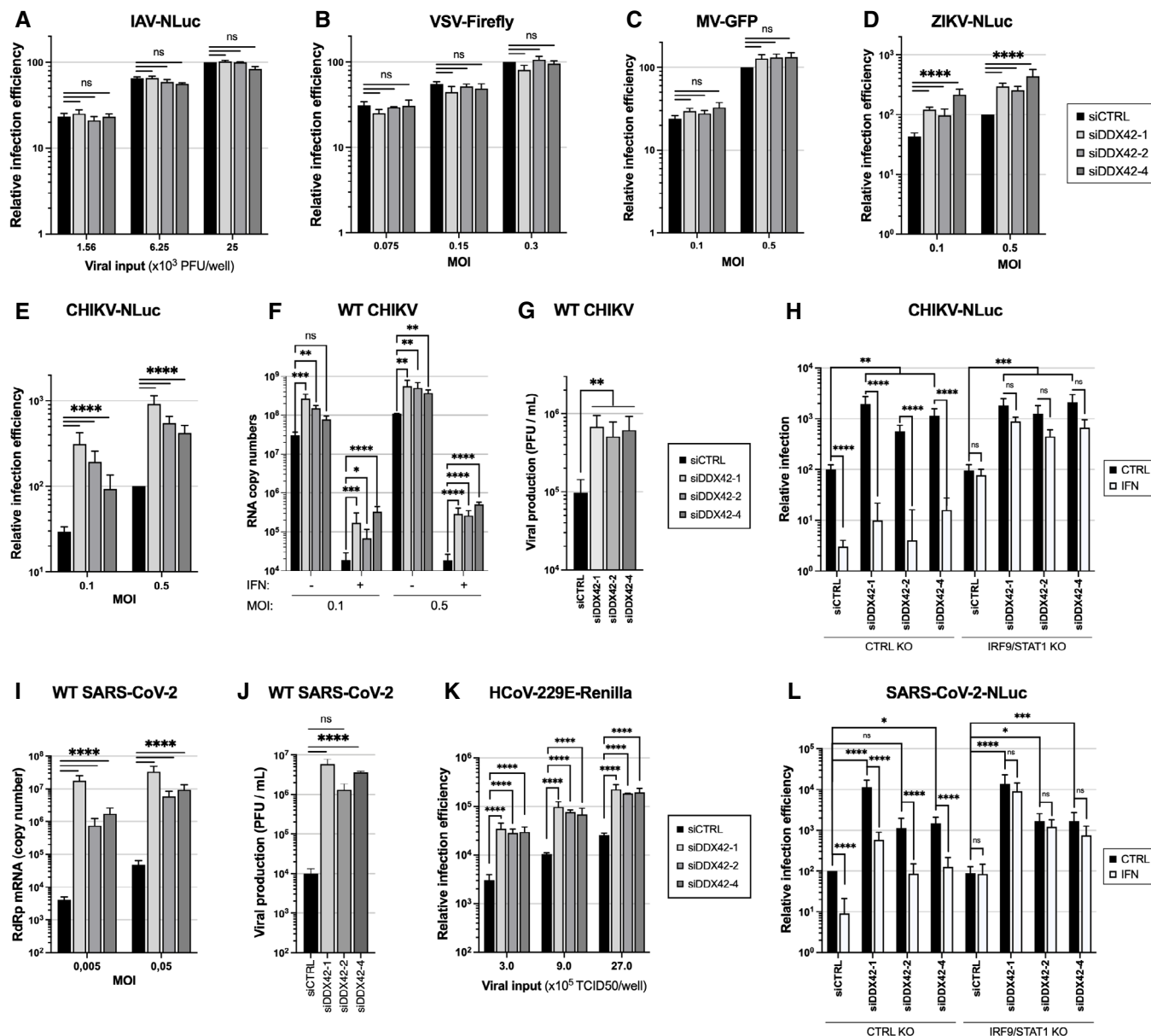


Figure 4.

DDX42 had a modest but significant, positive impact on ZIKV replication in U87-MG cells, as measured with a Nanoluciferase reporter virus (Fig 4D), whereas the impact was minor on WT ZIKV infection in Huh-7 cells, as measured by monitoring the percentage of cells expressing the viral protein E (Fig EV4B). To determine whether this was due to the lower silencing efficiency in Huh-7 cells compared with U87-MG cells (Fig EV4A) or to the use of reporter versus WT viruses, we repeated these experiments in U87-MG cells infected with WT ZIKV and assessing viral RNA yield by RT-qPCR analysis (Fig EV4C). This confirmed a minor (~ 2-fold) but nonetheless significant impact of DDX42 depletion on WT ZIKV replication. Noteworthy, when cells were pre-exposed to IFN prior to infection, DDX42 depletion had a stronger positive impact on ZIKV replication (~ 6.5-, ~ 4.5-, and 7-fold increase in infection efficiency with siDDX42-1, -2, and -4, respectively, compared with siCTRL;

Fig EV4C). DDX42 was proposed to play a role in the IFN responses against another flavivirus, Japanese encephalitis virus (JEV) (Lin *et al*, 2008). Indeed, a carboxyl-terminal fragment of DDX42 was identified as a partner of JEV protein NS4A and suggested to regulate IFN responses to this virus (Lin *et al*, 2008). However, the impact of endogenous DDX42 (or even ectopically expressed, full-length DDX42) on JEV replication had not been explored (Lin *et al*, 2008). Therefore, we analyzed the effect of DDX42 depletion on JEV replication. DDX42 depletion had no significant effect on JEV replication, unless cells had been pre-exposed to IFN (~ 1.8-fold effect without IFN, versus 4.3-, 2.3-, and 6.6-fold increase with siDDX42-1, 2 and -4, respectively, with IFN pre-treatment) (Fig EV4D). However, analyzing the expression of prototype ISGs by RT-qPCR showed that neither ZIKV nor JEV induced prototype ISG expression in U87-MG cells and that DDX42 did not substantially impact the

response to IFN (Fig EV4E). Of note, Regarding YFV and DENV-2 replication, DDX42 silencing had little to no effect on these viruses in Huh-7 cells, as measured by the percentage of cells positive for the viral protein E (Fig EV4F and G). In contrast, DDX42 depletion had a more profound effect on replication of a reporter CHIKV (Fig 4E) and WT CHIKV, as measured by RT-qPCR (Fig 4F) and plaque assays (Fig 4G). Contrary to what was observed with ZIKV and JEV (Fig EV4C and D) but reminiscent of HIV-1 data (Fig 2A and B), we observed that DDX42 depletion had a positive impact on CHIKV infection both in the absence and presence of IFN (Fig 4F). We then studied prototype ISG induction upon CHIKV replication in U87-MG cells, in the presence and absence of IFN and DDX42 (Fig EV4H). We did not observe ISG induction upon CHIKV replication, and DDX42 depletion had a minor impact on ISG induction upon IFN treatment, regardless of infection (e.g. 0.8 to 2-fold difference in OAS1 induction in the presence and absence of DDX42) (Fig EV4H). Next, we took advantage of the IRF9/STAT1 double KO U87-MG/CD4/CXCR4 cell populations, which were severely impacted in their ability to respond to IFN (Fig EV2E). In these cells, similarly to what was observed for HIV-1, DDX42 depletion had an identical, positive impact on CHIKV infection than in control KO cells (Fig 4H), confirming that DDX42's antiviral activity was not dependent on the IFN response. Next, we studied the impact of DDX42 on two coronaviruses and observed that the replication of SARS-CoV-2 (Fig 4I and J) and HCoV-229E (Fig 4K) were highly impacted by DDX42 depletion (up to 3 log-increase with SARS-CoV-2 as measured by RT-qPCR or plaque assays, Fig 4I and J, respectively, and up to 1 log-increase in infection efficiency with HCoV-229E-Renilla, Fig 4K; silencing efficiencies in the different cell lines used are shown in Fig EV4A). In agreement with this, DDX42 was recently identified as a potential inhibitor of SARS-CoV-2 replication in a whole-genome CRISPR screen in simian cells (Wei *et al.*, 2020). Finally, to test the importance of IFN signaling in DDX42's anti-SARS-CoV-2 activity, we generated IRF9/STAT1 double KO A549-ACE2 cell populations, which were unable to respond to IFN (Fig EV4I). As previously observed with HIV-1 and CHIKV, DDX42 depletion had a similar impact in these cells than in control KO cells (Fig 4L). Together, this showed that DDX42 did not rely on IFN responses for exerting its antiviral activity against HIV-1, CHIKV and SARS-CoV-2, while IFN pre-treatment seemed to slightly increase the impact of DDX42 on ZIKV and JEV flaviviruses. This might be due to the fact that some flavivirus-specific ISG(s) may help, or act in favor of, DDX42's antiviral activity. For instance, some ISG(s) may render the replication complexes more accessible

to DDX42. Alternatively, the decrease in infection efficiency by IFN might indirectly favor DDX42's antiviral activity.

DDX42 is found in close proximity to viral components and interacts with viral RNAs

In order to explore the impact of DDX42 on SARS-CoV-2 replication, we used PLA to determine whether DDX42 was in the vicinity of viral components in infected A549-ACE2 cells. To this aim, PLA was performed with either an anti-double strand (ds)RNA or an anti-Nucleoprotein (N) antibody, together with an anti-DDX42 antibody, followed by immunofluorescence staining to identify the infected cells (Fig 5A and B). In the latter, there was a significantly higher number of dsRNA-DDX42 and N-DDX42 PLA punctae than in control cells. This proximity suggested a potential interaction between DDX42 and SARS-CoV-2 viral components. To test whether DDX42 RNA helicase could interact with viral RNAs in infected cells, cross-linking RNA immunoprecipitation experiments were conducted following viral infection of U87-MG cells expressing either Flag-DDX42 or negative control Flag-Firefly (in addition to ACE2 for SARS-CoV-2 infection) (Fig 5C–E). A significant enrichment of the viral RNAs recovered with Flag-DDX42 immunoprecipitation was observed in comparison to the negative control for the sensitive viruses SARS-CoV-2 and CHIKV (Fig 5C and D), but not for IAV, which was insensitive to DDX42 antiviral activity (Figs 4A and 5E). Interestingly, DDX42 was recently shown to interact with RNAs presenting secondary structures, such as dsRNA (Pennemann *et al.*, 2021) and G4-quadruplexes (G4s) (Zyner *et al.*, 2019). G4s are secondary structures found both in cellular and viral nucleic acids and involved in various processes (e.g. transcription, translation or replication), and various viral genomes are known to possess such structures (Fay *et al.*, 2017; Ruggiero & Richter, 2018). To confirm the ability of DDX42 to bind structured RNAs (Zyner *et al.*, 2019; Pennemann *et al.*, 2021), we performed pull-down experiments using recombinant DDX42 (Fig EV3B) and several types of biotinylated RNAs: polyinosinic-polycytidylic acid (poly(I:C)), a predicted G4 found in CHIKV genomic RNA using G4Hunter (Bedrat *et al.*, 2016; Lacroix, 2019), a G4 present in TRF2 cellular mRNA (Lavigne *et al.*, 2021), as well as a negative control (i.e. TRF2 sequence bearing mutations and therefore unable to fold into G4s; Lavigne *et al.*, 2021) (Fig 5F). We observed that DDX42 indeed interacted with poly(I:C) and with the predicted G4 from CHIKV and TRF2 G4, but not with the negative control RNA. This experiment confirmed DDX42's ability to bind to structured RNAs but not to the unstructured, control RNA (Fig 5F).

Figure 5. DDX42 is found in close proximity to viral components and interacts with viral RNAs.

- A, B (A) Left, A549-ACE2 cells were infected or not with SARS-CoV-2 for 24 h prior to PLA using mouse anti-dsRNA (J2) and rabbit anti-DDX42 antibodies, followed by additional immunofluorescence (IF) staining with anti-mouse Alexa Fluor 546 antibody (PLA in green, IF in magenta). Representative Z-stack projection images are shown; scale bar: 15 μ m. Right, Average punctae were quantified in 3 biological replicates with mean \pm SD ($n > 75$ cells per condition). Mann-Whitney test. (B) Identical to A but using an anti-N antibody instead of anti-dsRNA antibody.
- C–E (C) Left, Quantification of SARS-CoV-2 RNA by RT-qPCR in RNA from total U87-MG-ACE2 cell lysates (input) and in Flag-Firefly (negative control) and Flag-DDX42 immunoprecipitation (IP). Multiple linear regression analysis on log-transformed data. Right, Percentage of immunoprecipitated RNA. Paired t-test on log-transformed data. (D) Identical to C following CHIKV infection of U87-MG cells. (E) Identical to C following IAV infection of U87-MG cells.
- F The following biotinylated RNAs were used to pull-down recombinant DDX42 (Fig EV3B): poly(I:C), CHIKV G4, TRF2 G4 and a mutated TRF2 G4 sequence (Mut. TRF2 G4), and DDX42 was revealed by an immunoblot. A representative experiment out of 2 biological replicates is shown.

Data information: (A–E) Data represent the mean \pm S.E.M. of 3 biological replicates. *P* values are denoted as follow: ns, not significant, **P* < 0.05, *****P* < 0.0001.

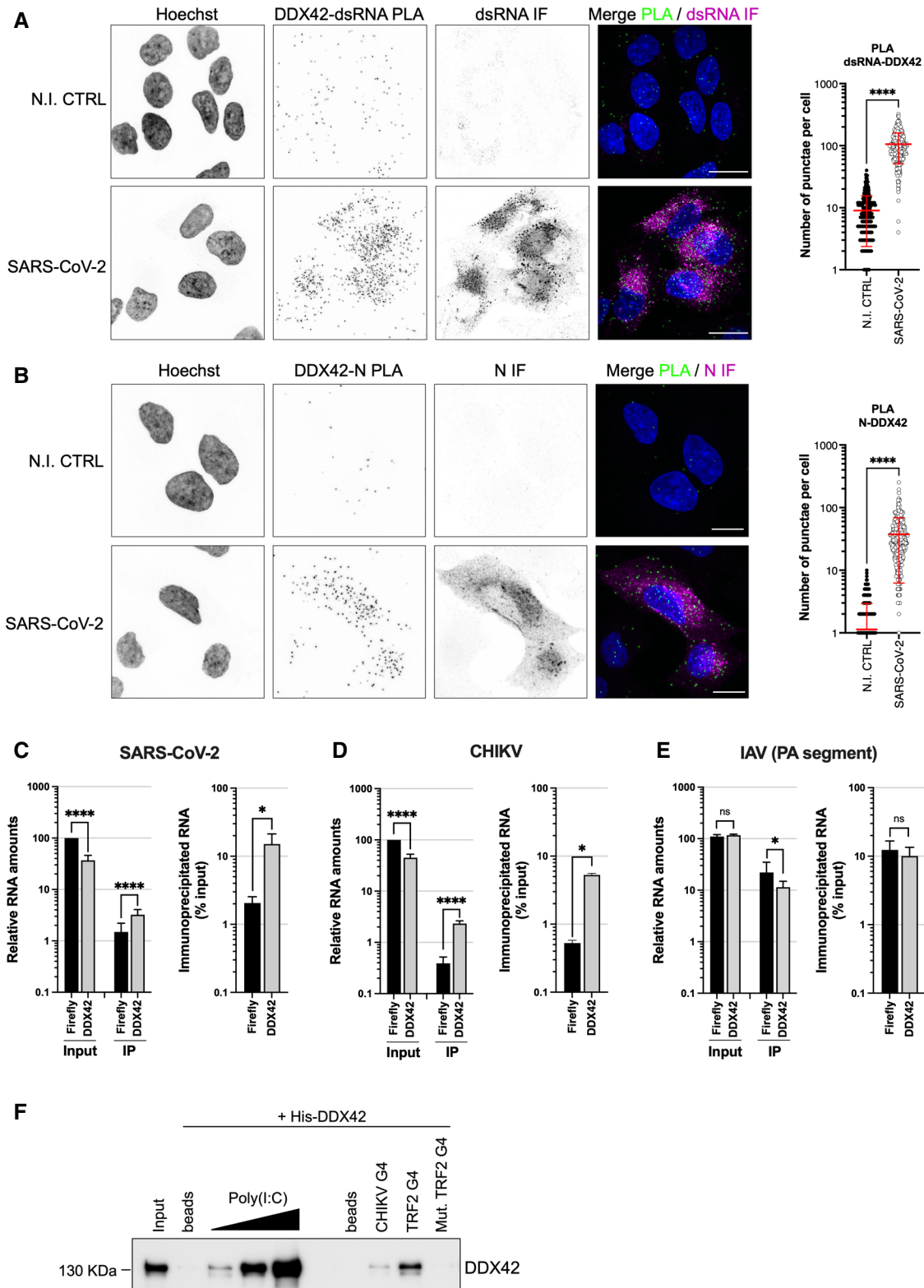


Figure 5.

DDX42 depletion does not have a global impact on the cellular transcriptome

As mentioned above, DDX42's lack of effect on negative strand RNA viruses (Fig 4A–C) argued against a global, indirect impact on the target cells. To confirm this, we performed RNA-seq analysis on siRNA-treated U87-MG and A549-ACE2 cells. The results showed that DDX42 depletion did not have a substantial impact on global cellular RNA expression (Dataset EV1 and Fig EV5). Of note, only 63 genes were commonly found differentially expressed upon DDX42 depletion with the 3 different siRNAs in U87-MG cells, and only 23 differentially expressed genes (DEGs) were identified in common in U87-MG and A549-ACE2 cells (Fig EV5A). Importantly, no known restriction factors were identified among the common DEGs (Dataset EV1), which strengthens the hypothesis that DDX42 may have a direct antiviral effect. Pathway analyses on the common DEGs and the other DEGs (i.e. not commonly regulated between the 3 siRNAs) additionally showed that all siRNA tested induced a similar effect within a cell type (Fig EV5B and C). Interestingly, median log₂ fold change of each pathway was lower than 0.6, suggesting a weak effect of DDX42 depletion on cell function (Fig EV5B and C).

Although not formerly proving it, taken together, our data strongly suggested that the DEAD-box RNA helicase DDX42 directly impacted viral replication. Indeed, our PLA assays showed a close proximity between DDX42 and HIV-1 Capsid, which is a viral protein recently shown to remain associated with reverse transcription complexes until proviral DNA integration in the nucleus (Peng *et al*, 2014; Burdick *et al*, 2020; Dharan *et al*, 2020). We also observed a close proximity between DDX42 and SARS-CoV-2 N or dsRNA, which could be suggestive of a potential interaction of DDX42 with viral components. In line with this, LINE-1 RNAs, as well as SARS-CoV-2 and CHIKV RNAs (but not IAV RNAs), were specifically pulled-down with DDX42. Interestingly, DDX42 is known to be a non-processive helicase, which also possesses RNA annealing activities and the ability to displace RNA-binding proteins from single-stranded RNAs (Uhlmann-Schiffler *et al*, 2006). Using recombinant DDX42, we showed that this helicase is capable of inhibiting HIV-1 reverse transcription *in vitro*. Moreover, we confirmed that DDX42 efficiently binds to dsRNA (as recently demonstrated while this manuscript was under revision; Pennemann *et al*, 2021) as well as G4s (Zyner *et al*, 2019). The functional relevance of this ability to bind G-quadruplexes is currently unknown. Viral genomes harbor numerous highly structured elements, such as G4s (Ruggiero & Richter, 2018), that could be involved in DDX42's antiviral activity. It will be of high interest to identify DDX42's determinants for viral RNA-binding activity and map the potential specific motifs or secondary structures preferentially bound by this helicase. Of note, DDX42 was initially identified, through mass spectrometry experiments, as a transient interactant of the spliceosome component SF3b, and had been proposed to play a role in RNP remodeling in this context, but this was not experimentally tested (Will *et al*, 2002). Whether DDX42 actually plays a role in the splicing machinery formation, or in any other cellular function(s), remains therefore to be assessed. A better understanding of DDX42 cellular functions may help uncover the mechanism by which it restricts viral replication. Based on the currently known activities of DDX42 and our data, one can envisage that it could bind to viral secondary RNA structures and/or affect viral RNP remodeling activities, impeding

viral replication (Will *et al*, 2002; Uhlmann-Schiffler *et al*, 2006). However, an indirect mode of action of DDX42 on viral replication cannot formerly be excluded and further work will be necessary to firmly decipher its mode of action.

DEAD box RNA helicases are well-known to participate in innate immunity, with some of the best examples being RIG-I-like receptors, which play an essential role in viral nucleic acid sensing. While also being involved in various cellular functions, some RNA helicases are involved in regulating (either positively or negatively) innate immune signaling. Other RNA helicases are well-known inhibitors of viruses and/or retroelements, like MOV10 for instance. Importantly, the expression of these RNA helicases can generally be IFN-regulated (Taschuk & Cherry, 2020; Bonaventure & Goujon, 2022). In contrast, there is very few known examples of RNA helicases with antiviral effector activities, which act independently of IFN. To our knowledge, so far, in addition to DDX42, a few helicases have been shown to possess such intrinsic antiviral functions. DDX17 is active against negative strand RNA bunyaviruses, through binding of viral RNA secondary structures, and this activity seemed conserved in *Drosophila* and humans (Moy *et al*, 2014). DDX56 was identified as an alphavirus inhibitor able to bind secondary structures present on CHIKV RNAs (Taschuk *et al*, 2020). DDX60, a positive regulator of RIG-I sensing pathway (Miyashita *et al*, 2011), was also shown to induce viral RNA degradation (Oshiumi *et al*, 2015). These RNA helicases and DDX42 are likely to ensure complementary functions by targeting different viruses, and/or by acting through distinct RNA-binding specificities. Nevertheless, DDX42's broad spectrum of action seems so far a rare feature among RNA helicases. Such a broad activity is reminiscent of other broadly-active antiviral inhibitors such as the MX1 GTPase (Haller *et al*, 2015). Further work will be warranted to explore in depth the breadth of DDX42 antiviral activity, especially in light of recent work showing that DDX42 inhibited a particular reporter strain of IAV in monocytic THP-1 cells (Pennemann *et al*, 2021). Interestingly, DDX42 showed a particularly strong antiviral activity against the beta-coronavirus SARS-CoV-2 and human seasonal alpha-coronavirus HCoV-229E. As these effects were greater than for most of the viruses tested, further characterization should be undergone to better understand DDX42 anti-coronavirus activity.

In conclusion, this work reveals DDX42 as a novel intrinsic antiviral inhibitor. Understanding the ability of this RNA helicase to control the replication of several positive-strand RNA viruses might contribute to the development of antiviral strategies.

Materials and Methods

Plasmids

The pLentiCas9-Blast, pLentiGuide-Puro vectors and the GeCKO sub-library A and B plasmids were a gift from Prof. F. Zhang (Addgene #52962, #52963, and #1000000048, respectively; Sanjana *et al*, 2014). LVs coding for sgRNAs targeting the candidate genes and control genes were obtained by cloning annealed oligonucleotides in BsmBI-digested pLentiGuide-Puro, as described (Addgene). Control sgRNAs and sgRNAs targeting the candidate genes, *MX2* and *IFNAR1*, were designed with the Optimized CRISPR Design tool (not available anymore), or with Chopchop (chopchop.

cbu.uib.no). The sgRNA coding sequences used were as follow: MX2 5'-CCGCCATTCGGCACAGTGCC-3', IFNAR1 5'-GACCCTAGTGCTCGTCGCCG-3', sgCTRL-1 5'-AGCACGTAATGTCCTGGAT-3', sgCTRL-2 5'-CAATCGGCGACGTTTTAAAT-3', sgCTRL-3 5'-TTAATTGGGTGGGCCCTGC-3', sgCTRL-4 5'-TTGGATATTAATTAGACATG-3', sgDDX42-1 5'-TCCTGAACCACACCAGCAGT-3', sgDDX42-2 5'-GGTGGTCTGGCACTAAGCG-3', sgDDX42-3 5'-AGGCACTGTGGGACTGCTGT-3', IRF9 5'-CGCTTTCAGTGTATTTACG-3', STAT1 5'-GCTTTCTAACCACTGTGC-3'. All the other sgRNA sequences are available upon request. In order to produce the HIV-1 based LVs used to perform the different steps of the screen (pRRL.sin.cPPT.CMV/NeomycinR.WPRE, pRRL.sin.cPPT.CMV/HygromycinR.WPRE and pRRL.sin.cPPT.CMV/ZeocinR.WPRE), neomycin, hygromycin and zeocin resistance genes (i.e. the genes coding for Neomycin phosphotransferase II, Hygromycin B phosphotransferase, and *Sh ble*) were amplified by PCR from pcDNA3.1 (ThermoFisher Scientific), pAHM (Goujon *et al*, 2013a), and pcDNA3.1/Zeo (ThermoFisher Scientific), respectively, and cloned by replacement of GFP in pRRL.sin.cPPT.CMV/GFP.WPRE (Goujon *et al*, 2008) using BamHI and SalI restriction sites. The pRRL.sin.cPPT.SFFV/E2-crimson-IRES-PuromycinR.WPRE has been described (Doyle *et al*, 2018). Human DDX42 cDNA was amplified by RT-PCR using the SuperScript IIITM (Invitrogen) from mRNAs of MDMs using primers DDX42-forward 5'-AATTAATTTAGGATCCATGAAGTGAATAAAGGTGGTCCTG and DDX42-reverse 5'-AATT AATTTACTCGAGCTAACTGTCCATCGACTTTTCTTGCG, and cloned by replacement of E2-crimson in BamHI-XhoI-digested pRRL.sin.cPPT.SFFV/E2-crimson-IRES-PuromycinR.WPRE, in order to obtain pRRL.sin.cPPT.SFFV/DDX42-IRES-PuromycinR.WPRE. The pRRL.sin.cPPT.SFFV/CD4-IRES-CXCR4.WPRE was obtained by replacement of E2-crimson-IRES-PuroR in pRRL.sin.cPPT.SFFV/E2-crimson-IRES-PuromycinR.WPRE with a BamHI/SalI fragment digested CD4-IRES-CXCR4 PCR fragment obtained from pMLV-CD4-IRES-CXCR4 (a gift from Prof. N. Sherer, Wisconsin University, USA). pRRL.sin.cPPT.SFFV/Firefly-IRES-PuromycinR.WPRE was obtained by amplification of Firefly by PCR from pGL4 (Promega) and cloned into BamHI-XhoI-digested pRRL.sin.cPPT.SFFV/E2-crimson-IRES-PuromycinR.WPRE. In some experiments, LVs without a selection marker were used: the IRES-PuromycinR cassette was removed by XhoI-SalI digestion and subsequent ligation, to obtain pRRL.sin.cPPT.SFFV/Firefly.WPRE and pRRL.sin.cPPT.SFFV/DDX42.WPRE. DDX42 K303E mutant was obtained by site-directed mutagenesis (by overlapping PCR using the aforementioned DDX42-forward and -reverse primers, respectively combined initially with reverse primer 5'-GGCTG CAGTTTCCCACTACCTGTTTGGCAATACC and forward primer 5'-GGTAGTGGGAAACTGCAGCCTTCATTTGGCC). pRRL.sin.cPPT.SFFV/ACE2.WPRE has been described (Rebendenne *et al*, 2021) (Addgene 145842). Flag-DDX42 and Flag-Firefly were amplified by PCR from the aforementioned LV plasmids and cloned into a NotI-XhoI-digested modified version of pCAGGS (Moncorge *et al*, 2013) to obtain pCAGGS/flag-DDX42.WPRE and pCAGGS/flag-Firefly.WPRE. The NL4-3/Nef-internal ribosome entry signal (IRES)-Renilla (NL4-3/Nef-IRES-Renilla) and the CCR5-version of this proviral clone (NL4-3/R5/Nef-IRES-Renilla) were gifts from Prof. Sumit Chanda (Goujon *et al*, 2013b). Wild-type and Ba-L Env bearing HIV-1 NL4-3, IIIB and HIV-2 proviral clones have been described (Adachi *et al*, 1986; Simon *et al*, 1995; Schaller *et al*, 2011), as well as the transmitted founder HIV-1 molecular clones CH077.t, CH106.c, REJO.c (gifts from Prof. B.

Hahn; Ochsenbauer *et al*, 2012) and HIV-2_{ROD10} and SIV_{MAC239} (Ryan-Graham & Peden, 1995; Gaddis *et al*, 2004). GFP-coding HIV-1 based LV system (i.e. p8.91 HIV-1 Gag-Pol, pMD.G, and GFP-coding minigenome), and HIV-2, FIV, and EIAV-derived, GFP coding LVs, as well as MLV-derived, GFP coding retroviral vectors have all been described (Naldini *et al*, 1996; Bainbridge *et al*, 2001; O'Rourke *et al*, 2002; Saenz *et al*, 2005). The LINE-1 plasmid 99 RPS-GFP PUR (pRPS-GFP), 99 RPS-GFP JM111 PUR (pJM111) and pLRE3-GFP were developed by Prof. Kazazian's lab (Moran *et al*, 1996; Ostertag *et al*, 2000; Goodier *et al*, 2012). pBlaM-Vpr and pAdvAntage have been described (Cavrois *et al*, 2002).

Cell lines

Human cell lines HEK293T (ATCC CRL-3216), A549 (ATCC CRM-CCL-185) were obtained from the ATCC, and U87-MG (ARP-2188) and TZM-bl (ARP-8129) from the AIDS reagent program. T98G cells were a gift from Prof. G. Kochs (Freiburg University, Germany; ATCC CRL-1690), MDCK cells a gift from Prof. W. Barclay (Imperial College London, UK), Vero E6 cells (Merck) were a gift from Christine Chable (CEMIPAI, CNRS, France), respectively, Huh7.5.1 cells have been described (Zhong *et al*, 2005) and provided by Raphaël Gaudin (IRIM, CNRS, France). Human hepatocellular carcinoma Huh-7 cells (Nakabayashi *et al*, 1982) were kindly given by Annette Martin (Institut Pasteur, Paris, France). These cell lines were cultured in Dulbecco's Modified Eagle Medium (DMEM) supplemented with 10% fetal bovine serum and 1% penicillin-streptomycin (ThermoFisher). T98G/Cas9 and U87-MG/Cas9 were obtained by transduction of T98G and U87-MG, respectively, with HIV-1-based LVs expressing the spCas9-P2A-Blasticidin cassette (pLentiCas9-Blast; Sanjana *et al*, 2014). U87-MG/CD4/CXCR4 have been described (Goujon *et al*, 2013a) and were further modified to express Cas9 and Firefly using pLentiCas9-Blast and pRRL.sin.cPPT.SFFV/Firefly.WPRE, respectively. T98G/Cas9/CD4/CXCR4/Firefly were obtained by successive transductions of T98G/Cas9 with pRRL.sin.cPPT.SFFV/CD4-IRES-CXCR4.WPRE at a high MOI, and pRRL.sin.cPPT.SFFV/Firefly.WPRE, at a low MOI, respectively. Cell surface staining with anti-CD4 and CXCR4 antibodies (Miltenyi Biotec) confirmed that more than 95% cells were positive for both markers. A549 cells stably expressing ACE2 were generated by transduction with RRL.sin.cPPT.SFFV.ACE2.WPRE containing-vector.

For antibiotic selection, cells were treated with 10 µg/ml Blastidicin (InvivoGen), 1 mg/ml Zeocin (InvivoGen), 2 µg/ml Puromycin (Sigma-Aldrich), 250 µg/ml Hygromycin (Sigma-Aldrich), 1 mg/ml G418 (Sigma-Aldrich). When indicated, universal type 1 IFN (PBL Interferon Source) was added at 1,000 U/ml for 16–24 h prior to virus infection or RNA extraction, and AZT and 3TC (AIDS reagent program) at 10 µM for 2 h prior to infection.

Primary cells

Blood from healthy donors was obtained from the Etablissement Français du Sang, under agreement 21PLER2019-0106. Peripheral blood mononuclear cells (PBMCs) were isolated by centrifugation through a Ficoll[®] Paque Plus cushion (Sigma-Aldrich). Primary human CD4⁺ T cells and monocytes were purified by positive selection using CD3 and CD14 MicroBeads, respectively (Miltenyi Biotec), as previously described (Goujon *et al*, 2013a). Monocytes

were incubated for 3 h in serum-free Roswell Park Memorial Institute (RPMI) 1640 medium and further differentiated into macrophages by culture for 5–7 days in RPMI 1640 supplemented with 10% fetal calf serum, 1% penicillin–streptomycin and 100 ng/ml granulocyte-macrophage colony-stimulating factor (GM-CSF; Miltenyi). CD4⁺ T cells were cultured in RPMI supplemented with 10% fetal bovine serum and 1% penicillin–streptomycin, and stimulated for 48 h with 10 µg/ml phytohemagglutinin (PHA) (Fisher Scientific) and 50 U/ml interleukin-2 (IL-2, Miltenyi Biotec) prior to electroporation.

Genome-scale CRISPR/Cas9 screens

The plasmids coding GeCKO sub-libraries A and B were amplified and prepared according to the provided guidelines (Lentiviral Crispr Toolbox, Addgene). 60 million T98G/Cas9 cells were transduced with GeCKO LVs at a MOI of 0.1 to cover about 100-times the half-library complexity. After 48 h, the cells were selected with puromycin, amplified for 12–15 days. 45 million cells were harvested and frozen down at –80°C for subsequent genomic DNA extraction, using the QIAamp DNA Blood Maxi Kit according to manufacturer's instructions (Qiagen). In parallel, 60 million cells from the initial GeCKO populations were used for the screen. The cells were treated with 1,000 U/ml IFN for 24 h, infected with LVs coding a hygromycin resistance cassette. 48 h later the cells were selected with hygromycin and the surviving cells amplified. Two other rounds of IFN treatment, LV infection and antibiotic selection were subsequently performed with LVs coding a neomycin resistance cassette and a zeocin resistance cassette, respectively. The three time-selected populations were amplified and 45 million cells were harvested and stored at –80°C for subsequent genomic DNA extraction, as previously. After genomic DNA extraction, the sgRNA coding sequences integrated in the genomic DNA from the initial and 3-times selected populations were amplified by touch-down PCR and sequenced by Illumina deep sequencing. To this aim, 120 µg of genomic DNA was amplified using DNA Herculase II Fusion DNA polymerase (Agilent) in the presence of 2% DMSO, 1 mM of dNTPs, and 400 nM of the following primers: Forward-primer1: 5'-TCGTCGGCAGCGTCAGATGTGTATAAGAGACAGCTTGTGGAAAGGACGAAACACC-3' for screen A or Forward-primer2: 5'-TCGTCGGCAGCGTCAGATGTGTATAAGAGACAGGATCTTGTGGAAAGGACGAAACACC-3' used for screen B, together with reverse primer: 5'-GTCTCTGGGCTCGGAGATGTGTATAAGAGACAAAGGTCCATTAGCTGCAAAGATTCTCTC-3'. Briefly, after 5 min at 95°C, 14 cycles of pre-amplification were performed with a hybridization temperature decreasing by 0.5°C per cycle (30 s at 95°C, 30 s at 60°C, and 30 s at 72°C), followed by 30 cycles of amplification (30 s at 95°C, 30 s at 53°C, and 30 s at 72°C). A 50 ng of each amplicon was dual indexed in a 5-cycle PCR reaction using the PCR module and indexed primers from the Nextera kit (Illumina). Resulting libraries were purified on AMPure XP magnetic beads (Beckman Coulter) using a 0.8× ratio and verified on Fragment Analyzer using the HS NGS fragment kit (Agilent). Libraries were quantified using microfluorimetry (QuBit, Invitrogen), mixed with a PhiX library (Illumina) and sequenced on one single read 50 nt lane of HiSeq2500 using the rapid mode.

Image analyses and base calling were performed using the Illumina HiSeq Control Software and Real-Time Analysis component (v1.18.66.3). Demultiplexing was performed using Illumina's conversion software (bcl2fastq 2.20). The quality of the raw data was

assessed using FastQC (v0.11.5) from the Babraham Institute and the Illumina software SAV (Sequencing Analysis Viewer). Potential contaminants were investigated with the FastQ Screen (Wingett & Andrews, 2018) (v0.11.4) software from the Babraham Institute.

Sequencing reads were trimmed using Cutadapt (Martin, 2011) (v1.13), with options -g [primer sequence] -u [length of remaining 3' bases] -e 0.2 -m 18 -l 20, to remove primer sequences and retrieve the 20 bases long sequences corresponding to sgRNAs. These retrieved sequences were then aligned to the GeCKOv2 Human Library (A or B) reference sequences (keeping only non-duplicated sgRNA sequences, the duplicated ones being annotated) using Bowtie (Langmead *et al*, 2009) (v1.2), with options -v 2 -norc -S. Resulting bam files were sorted and indexed using Samtools (Li *et al*, 2009) (v1.5). Quantification of sgRNAs was done using Samtools idxstats. MAGeCK (Li *et al*, 2014) (v0.5.7) was used to normalize (total count method) and identify enriched sgRNAs and genes in 3-times selected cell populations versus starting GeCKO transduced cells (mageck test command).

Lentiviral and retroviral production

To produce lentiviral vector particles, HEK293T cells were transfected by polyethylenimine (PEI) co-transfection with miniviral, HIV-1 based genome coding plasmids (e.g. LentiCas9-Blast, LentiGuide-Puro or pRRL-SFFV), p8.91 (HIV-1 GagPol) and pMD.G (VSV-G) at a ratio of 1:1:0.5, respectively. The medium was replaced after 6 h and viral particles were harvested 42 h later, filtered, and directly used to transduce target cells (or stored at –80°C). After 4 to 6 h, the transduction medium was replaced with complete DMEM, and the cells were treated 48 h later with the relevant antibiotics. The HIV-2-, FIV-, EIAV-GFP coding LVs were produced using GFP-coding HIV-2-, FIV-, EIAV-based miniviral genomes, together with HIV-2-, FIV-, EIAV- GagPol, expression constructs and pMD.G at a ratio of 1:1:0.5. MIGR1 MLV-derived retroviral vectors were obtained with B-MLV Gag-Pol-expressing plasmid pCIG3B, the GFP-expressing minigenome pMIGR1 and pMD.G. at a ratio of 1:1:0.5, respectively and harvested as previously described.

HIV-1 Renilla and NL4-3 HIV-1 were produced by standard PEI transfection of HEK293T. When indicated, pMD.G was cotransfected with the provirus at a 3:1 (provirus:MD.G) ratio. The culture medium was changed 6 h later, and virus-containing supernatants were harvested 42 h later. Viral particles were filtered, purified by ultracentrifugation through a sucrose cushion (25% weight/volume) for 75 min at 4°C and 133,000 g using a SW 32 TI rotor (Beckman Coulter), resuspended in serum-free RPMI 1640 or DMEM medium and stored in small aliquots at –80°C. Viral particles were titrated using an HIV-1 p24^{Gag} Alpha-Lisa kit and an Envision plate reader (Perkin Elmer) and/or by determining their infection titers on target cells.

β-lactamase-Vpr (BlaM-Vpr)-carrying viruses, bearing the wild-type Env, were produced by co-transfection of HEK293T cells with the NL4-3/Nef-IRES-Renilla provirus expression vector, pBlaM-Vpr and pAdvantage at a ratio of 4:1:0.5, as previously described (Cavrois *et al*, 2002). Viral particles were titrated using an HIV-1 p24^{Gag} Alpha-Lisa kit and an Envision plate reader (Perkin Elmer).

Lentiviral and retroviral infections

For infections with replication-competent HIV-1 Renilla or wild-type and/or VSV-G pseudotyped-HIV-1, target cells were plated at

2.5×10^4 cells per well in 96-well plates or at 2×10^5 cells per well in 12-well plates and infected for 24–48 h before lysis and Renilla (and Firefly) luciferase activity measure (Dual-Luciferase[®] Reporter Assay System Promega) or fixation with 2% paraformaldehyde (PFA)-PBS, permeabilization (Perm/Wash buffer, BDBiosciences) and intracellular staining with the anti-p24^{Gag} KC57-FITC antibody (Beckman Coulter), as described previously (Goujon & Malim, 2010). For TZM-bl assays, the β -galactosidase activity was measured using the Galacto-Star[™] system (ThermoFisher Scientific). For infections with lentiviral and retroviral vectors, target cells were plated at 2.5×10^4 cells per well in 96-well plates the day prior to infection with vectors at the indicated MOIs, and the percentages of infected cells were scored by flow cytometry 24 h later. For primary CD4⁺ T cell infections, 10^5 cells were infected with 100 ng p24^{Gag} of HIV-1 Renilla for 24 h prior to lysis and luciferase activity measure. For MDM infections, 8×10^4 cells were infected with 100 ng p24^{Gag} of a CCR5-tropic version of HIV-1 Renilla for 30 h prior to lysis and luciferase activity measure.

Retrotransposon assays

For GFP-based retrotransposon assays, HEK293T cells (2×10^5 cells) were co-transfected with either 1 μ g of pJM111 (a negative control with two point mutations in ORF1 that abolish retrotransposition), pRPS-GFP or pLRE3-GFP with either 1 μ g of pCAGGS-Flag-Firefly or pCAGGS-Flag-DDX42. At 7 days post-transfection, the percentage of GFP-expressing cells was scored by flow cytometry.

CRISPR/Cas9 knock-out

For CRISPR/Cas9 knock-out in cell lines, Lentiguide-Puro LVs coding sgRNAs targeting the indicated genes or non-targeting sgRNAs were produced, and U87-MG Cas9/CD4/CXCR4/Firefly were transduced for 6 h before replacing the supernatants with fresh, complete medium. The transduced cells were selected with puromycin 2 days later and amplified for 12–15 days. For CRISPR/Cas9 knock-out in activated primary CD4⁺ T cells, 2 million cells per condition were washed with PBS1X, and electroporated using the 4d-Nucleofector[®] (Lonza) and the Amaxa P3 primary cell kit with 183 pmol of crispR-tracr RNA duplex (Alt-R CRISPR-Cas9 crRNA XT and tracrRNA XT, IDT[®]) and 61 pmol of Cas9 (Alt-R[®] S.p. Cas9 Nuclease V3, IDT[®]). After electroporation, the cells were incubated for 4 days at 37°C in X-VIVO15 medium (Lonza) supplemented with 1% pen/strep and IL-2 at 500 U/ml prior to cell counting and infection. The crRNA sequences of the sgDDX42-1, -2, and -3 were identical to the ones cloned in pLentiguide-Puro, and the crRNA of the sgDDX42-4 and sgDDX42-5 were pre-designed by IDT[®], as follow: sg4-DDX42 5'-CGGAGATCTATTAAGTCTG-3', sg5-DDX42 5'-GAGTTGGTGAGTTTTCAGC-3'.

siRNA transfection

DDX42 and control knockdowns were achieved by transfecting the indicated siRNAs at 44, 14.2, and 100 nM final in U87-MG and Huh-7 cells, TZM-bl cells and MDMs, respectively, with lipofectamine RNAimax (ThermoFisher Scientific) according to the manufacturer's instructions. The scramble siRNA controls used were universal siCTRL1 (SIC001) and siCTRL2 (SIC002) (Sigma-Aldrich) and the

sequences of the siRNAs targeting DDX42 were siDDX42-1: 5'-CAGAAUGCCUGUUUCGGA-3' (SASI_Hs01_00119846, Sigma-Aldrich[®]), siDDX42-2: 5'-CUUACCUUGUGUUUGAUGA-3' (SASI_Hs01_00119845, Sigma-Aldrich[®]), siDDX42-4: 5'-AUCUCGAAUACCCUUUACG-3' (ID: 136410, Ambion[®]).

Cell viability assays

Cell viability was assessed in siRNA-transfected cells by measuring cellular ATP levels 72 h post-transfection using the CellTiter-Glo[®] Luminescent Cell Viability Assay kit (Promega) according to manufacturer's instructions.

BlaM-Vpr assay for HIV-1 entry

This assay was performed as described previously (Goujon & Malim, 2010). Briefly, 2×10^5 U87-MG/CD4/CXCR4 cells were plated in 24-well plates and incubated with BlaM-Vpr carrying NL4-3 particles (31, 62, 125 ng p24^{Gag}) or mock-infected for 3 h at 37°C. The cells were then washed once in CO₂-independent medium and loaded with CCF2-AM substrate-containing solution (ThermoFisher Scientific) for 1 h at room temperature before 2 washes and incubation at room temperature for 16 h in development medium (CO₂-independent medium containing 2.5 mM probenecid). Finally, the cells were trypsinized, washed and fixed in 1% PFA-PBS1X before analysis with a FACSCanto[™] II (Becton Dickinson).

Cross-linking RNA immunoprecipitation

For LINE-1 RNA immunoprecipitation, HEK293T cells were co-transfected with equal amounts of pRPS-GFP and pCAGGS-Flag-DDX42 or -Flag-Firefly. For viral RNA immunoprecipitation, U87-MG cells were transduced with either Flag-Firefly or Flag-DDX42 coding lentiviral vectors (pRRL.sin.cPPT.SFFV/Flag-Firefly.WPRE and pRRL.sin.cPPT.SFFV/Flag-DDX42.WPRE, respectively) and infected with CHIKV at MOI 0.1, SARS-CoV-2 at MOI 0.13, or A/Victoria/3/75 IAV at MOI 0.1 for 24 h. 4 days post LINE-1-transfection or 24 h post-infection, cells were washed twice in PBS1X, incubated for 10 min with 0.1% formaldehyde in PBS1X, for 5 min in 250 mM Glycine and washed twice in cold PBS1X. Cells were lysed in RIPA buffer (50 mM Tris/HCl pH 7.5, 150 mM NaCl, 1% NP-40, 0.5% sodium deoxycholate, 1 mM EDTA, protease inhibitor cocktail and 40 U/ml RNasin). The lysates were clarified by centrifugation at 16,000 g, for 10 min at 4°C. Fractions of cell lysates were harvested at this stage to serve as controls for protein and RNA inputs (15%) and the rest was incubated with Flag-magnetic beads (ThermoFisher Scientific) for 2 h at 4°C. The beads were washed 5 times in RIPA buffer and the immunoprecipitated proteins eluted using 150 μ g/ml 3 \times Flag peptide (Sigma-Aldrich) in elution buffer (50 mM Tris/HCl pH 7.5, 75 mM NaCl, 1 mM DTT, protease inhibitor cocktail and 40 U/ml RNasin) for 2 h. Fractions of eluates were harvested for immunoblot analysis (1/6th) and the rest subjected to RNA extraction (5/6th). RNA extractions were then performed using TRIzol (ThermoFisher Scientific).

RNA quantification by RT-qPCR

To check silencing efficiency or measure gene induction after IFN treatment, $0.5\text{--}2 \times 10^6$ cells were collected 2–3 days after siRNA

transfection or 24 h after IFN treatment or no treatment, and total RNAs were isolated using the RNeasy kit with on-column DNase treatment (Qiagen). cDNAs were generated using 250 ng RNA (High-Capacity cDNA Reverse Transcription Kit, Applied Biosystem, ThermoFisher Scientific, catalog number 4368814) and analyzed by quantitative (q)PCR using TaqMan gene expression assays (Applied Biosystem) specific for ACTB (Hs99999903_m1), GAPDH (Hs99999905_m1), DDX42 (Hs00201296_m1), ISG15 (Hs00192713_m1). Triplicate reactions were run according to the manufacturer's instructions using a ViiA 7 Real-Time PCR system. For relative quantification, samples were normalized to both ACTB and GAPDH mRNA expression and $\Delta\Delta C_t$ analysis was performed. For the RNA extraction and RT-qPCR analysis, specifically in Huh-7 cells, total RNAs were extracted from cell lysates using the NucleoSpin RNA II kit (Macherey-Nagel), following the manufacturer's protocol. Equal amounts of purified total RNA were used to synthesize first strand cDNA using random hexamers (Thermo Fisher) and the ReverAid H Minus Moloney murine leukemia virus (M-MuLV) reverse transcriptase (Thermo Fisher). Quantitative real-time PCR was performed on a real-time PCR system (Quant Studio 6 Flex from Applied Biosystems) with SYBR green PCR master mix (Life Technologies). Data were analyzed with the $\Delta\Delta C_t$ method. All the samples were analyzed in technical triplicates and normalized to GAPDH (glyceraldehyde-3-phosphate dehydrogenase) as endogenous reference control. The primer sequences used for Fig EV4A (Huh-7) were as follow: GAPDH Forward: 5'-GGTCGGAGTCAACGGATTTG-3', reverse: 5'-ACTCCACGACGTACTCAGCG-3'; DDX42 Forward: 5'-GGCTATACCTACTCACTCCC-3', reverse: 5'-CCACCAATGTTACAGCTTTTTTCC-3'.

For the measure of LINE-1 RNAs, 100 ng RNA (from cell extracts) or 25 μ l of RNA extracted from the IP eluates (i.e. ~ 60% of the total amount of immunoprecipitated RNA) were reverse transcribed and analyzed by qPCR using primers and probe specific for ORF2: ORF2-forward 5'-CACCAGTTAGAATGGCAATCATTA-3', ORF2-reverse 5'-GGGATGGCTGGTCAAATGG-3' with ORF2-probe 5'-[FAM]-AGGAAACAACAGGTGCTGGAGAGGATGC-[TAMRA]-3'. Absolute quantification was performed using a pRPS-GFP standard curve.

For the measure of SARS-CoV-2 replication, 3×10^5 cells were harvested and total RNA was extracted using the RNeasy kit (Qiagen) employing on-column DNase treatment. 125 ng of cellular RNAs were used to generate cDNAs that were analyzed by qPCR using RdRp primers and probe, as follow: RdRp_for 5'-GTGARATGTCATGTGTGGCGG-3', RdRp_rev 5'-CAAATGTAAA AACACTATTAGCATA-3', and RdRp_probe 5'-[FAM]-CAGGTGGA ACCTCATCAGGAGATGC-[TAMRA]-3' (Corman et al, 2020). pRdRp (which contains an RdRp fragment amplified from SARS-CoV-2-infected cell RNAs; Rebendenne et al, 2021) was diluted in 20 ng/ml salmon sperm DNA to generate a standard curve to calculate relative cDNA copy numbers and confirm the assay linearity (detection limit: 10 molecules of RdRp per reaction).

For ZIKV and JEV RNA quantification, total RNAs were extracted from cell lysates using the NucleoSpin RNA II kit (Macherey-Nagel), following the manufacturer's protocol. Equal amounts of purified total RNA were used to synthesize first strand cDNA using random hexamers (Thermo Fisher) and the ReverAid H Minus Moloney murine leukemia virus (M-MuLV) reverse transcriptase (Thermo Fisher). Quantitative real-time PCR was performed on a real-time

PCR system (Quant Studio 6 Flex from Applied Biosystems) with SYBR green PCR master mix (Life Technologies). The following primer sequences were used: ZIKV-Forw 5'-AARTACACATAC CARAACAAAGTGGT-3' and Rev 5'-TCCRCTCCCYCTYTGGTCTTG-3' (Lesage et al, 2022); JEV-Forw 5'-CGTGCAGAGGACAGGATGAG-3' and Rev 5'-AGACGCAAGTCCCTACGATG-3'.

For the measure of the amounts of viral RNAs in the RNA immunoprecipitation experiments, 100 ng RNA from cell lysates (input) or 25 μ l of RNA extracted from the IP eluates (i.e. ~ 60% of the total amount of immunoprecipitated) were reverse transcribed using the High-Capacity cDNA Reverse Transcription Kit as above. For SARS-CoV-2, the cDNAs were analyzed by RdRp RT-qPCR. For CHIKV RNA, the following primers and probe were used for the qPCR reactions: E1-C21-forward 5'-ACGCGATTGAGCGAAGCAC-3', E1-C21-reverse 5'-CTGAAGACATTGGCCCCAC-3' (Meertens et al, 2019), and E1-C21-probe 5'-[FAM]-CTCATACCGCATCTGCATCAGCTAAGCTCC-[TAMRA]-3'. pE1 (which contains an E1 fragment amplified from CHIKV-infected cell RNAs using primers E1-C21 forward and E1-C21 reverse and cloned into pPCR-Blunt II-TOPO) was used to generate a standard curve and ensure the linearity of the assay (detection limit: at least 10 molecules per reaction). For A/Victoria/3/75 IAV RNA, the following primers and probe, specific for the PA segment, were used, as follow: PA-forward 5'-TTGCTGCACAGGATGCATTA-3', PA-reverse 5'-AGATTGGAGAAG ACGTGGCT-3' and PA-probe 5'-[FAM]-TGGCTCTGCAATGGGACACCTCTGC-[TAMRA]-3'. pPoll-RT-Victoria-PA (Zürcher et al, 1996) was used to generate a standard curve and ensure the linearity of the assay (detection limit: at least 10 molecules per reaction).

Quantification of HIV-1 DNAs

To measure HIV-1 cDNAs, 2×10^5 cells transfected with a control siRNA or siRNAs targeting DDX42 were plated in 24-well plates, and treated or not with 10 μ M AZT and 3TC 1–2 h prior to infection. The cells were infected with NL4-3 HIV-1 (60 ng p24^{Gag}) for 2 h at 37°C, washed with PBS1X and incubated in complete DMEM before being harvested at the indicated times. Cell pellets were frozen at -80°C after two washes in PBS1X. Total DNA extraction was performed using the DNeasy kit (Qiagen) according to the manufacturer's instructions, and a DpnI-treatment step was performed prior to qPCR. Strong stop reverse transcription products were detected using forward primer oHC64 5'-TAACTAGGGAACCCACTGC-3' and reverse primer oHC65 5'-GCTAGAGATTTCCACACTG-3', 2nd strand transfer product using oHC64 and oSA63R 5'-CTGCGTGCAGAGATCTCCTCTGGCT-3', together with oHC66 probe 5'-[FAM]-ACACAACAGACGGGCACACACTA-[TAMRA]-3'. 2-LTR circular forms were detected using 2LTR-forward 5'-GTAAC TAGATCCCTCAG-3' and 2LTR-reverse 5'-TGGCCCTGGTGTGTAGTTC-3' together with 2LTR-probe 5'-[FAM]-CTACCACACAAGGCTACTTCCCTGAT-[TAMRA]-3'. Integrated viral DNA was analyzed using an Alu qPCR as described before (Goujon et al, 2013a). Briefly, a preamplification of 16 cycles was performed (15 s at 94°C, 15 s at 55°C, 100 s at 68°C) with Platinum Taq DNA High Fidelity polymerase (Invitrogen) using 100 nM of genomic Alu forward primer 5'-GCCTCCCAAAGTCTGGGATTACAG and 600 nM of U3-reverse primer 5'-CTTCTACCTTATCTGGCTCAAC-3'. The pre-amplification step was performed on serial dilutions of all the DNA

samples, as well as of a positive control (total DNA from U87-MG infected with a high input of NL4-3), to ensure the linearity of the assay. Background levels were assessed using linear, one-way amplification by performing the pre-amplification PCR with the U3-reverse primer alone. Then a qPCR was performed on pre-amplification products using U3-forward primer 5'-TCTACCACA CACAAGGCTAC-3' and U3-reverse primer with the U3 probe 5'-[FAM]-CAGAACTACACACCAGGGCCAGGGTCA-[TAMRA]-3'. qPCR reactions were performed in triplicates, in Universal PCR master mix using 900 nM each primer and 250 nM probe with the following program: 10 min at 95°C followed by 40 cycles (15 s at 95°C and 1 min at 60°C). pNL4-3 or pTOPO-2LTR (generated by pTOPO cloning of a 2-LTR circle junction amplified from NL4-3 infected cells, using oHC64 and U3-reverse primers into pCRTM2.1-TOPOTM) were diluted in 20 ng/ml of salmon sperm DNA to create dilution standards used to quantify relative cDNA copy numbers and confirm the linearity of all assays.

Proximity ligation assays (PLAs)

The proximity ligation assays were performed using the Duolink[®] *in situ* Detection Reagents (Sigma-Aldrich, DUO92014). For PLA with HIV-1, MDMs were plated in 24-well plates with coverslips pre-treated with poly-L-lysine (Sigma-Aldrich) and infected with 1 µg p24^{Gag} of HIV-1 NL4-3 (Ba-L Env) or mock-infected. For PLA with SARS-CoV-2, A549-ACE2 cells were plated in 24-well plates with coverslips and infected at an MOI of 0.1. 24 h later, the cells were fixed with 2–4% PFA in PBS1X for 10 min, washed in PBS1X and permeabilized with 0.2% Triton X-100 for 10 min. After a couple of washes in PBS1X, either NGB buffer (50 mM NH₄Cl, 2% goat serum and 2% bovine serum albumin in PBS) or Duolink[®] blocking solution was added for 1 h. Cells were incubated with mouse AG3.0 anti-HIV-1 Capsid antibody (National Institutes of Health (NIH) AIDS Reagent Program #4121), or J2 anti-dsRNA antibody (SCICONS), or anti-SARS-CoV-2 Nucleoprotein (N; BioVision), and rabbit anti-DDX42 antibody (HPA023571, Sigma-Aldrich) diluted in NGB buffer or in Duolink[®] blocking solution for 1 h. After 2 washes in PBS1X, the cells were incubated with the DUOLINK[®] *in situ* PLA[®] Probe Anti-rabbit minus (DUO92006) and DUOLINK[®] *in situ* PLA[®] Probe Anti-mouse plus (DUO92001) for 1 h at 37°C. After 2 washes in PBS1X, the ligation mix was added for 30 min at 37°C. After 2 washes in PBS1X, the cells were incubated with the amplification mix for 100 min at 37°C followed by 3 washes in PBS1X. In the case of SARS-CoV-2 infection, an additional staining was performed by incubating cells in an anti-mouse Alexa Fluor secondary antibody. Finally, the cells were washed twice with PBS1X and stained with Hoechst at 1 µg/ml for 5 min, washed again and the coverslips mounted on slides in Prolong mounting media (ThermoFisher Scientific). Z-stack images were acquired using an LSM 880 confocal microscope (ZEISS) using a 63× lens. Of note, sample names were coded and analyzed without blindly, i.e. knowledge of their identity. PLA punctae quantification was performed using the FIJI software (Schindelin *et al*, 2012). Briefly, maximum z-projections were performed on each z-stack and the number of nuclei per field were quantified. Then, by using a median filter and thresholding, PLA punctae were isolated and quantified automatically using the Analyze Particles function. To obtain a mean number of dots per cell, the number of PLA dots per field were averaged by

the number of nuclei. In the case of SARS-CoV-2 infection, the infected cells were identified using N or dsRNA immunofluorescence staining. For representative images, single cells were imaged using a LSM880 confocal microscope coupled with an Airyscan module. Processing of the raw Airyscan images was performed on the ZEN Black software.

Immunoblot analysis

Cell pellets were lysed in sample buffer (10 mM Tris-HCl pH7.6, 150 mM NaCl, 1% Triton X100, 1 mM EDTA, 0.1% deoxycholate, 2% SDS, 5% Glycerol, 100 mM DTT, 0.02% bromophenol blue), resolved by SDS-PAGE and analyzed by immunoblotting using primary antibodies specific for human DDX42 (HPA023571, Sigma-Aldrich; dilution 1/300), Flag (M2, Sigma-Aldrich; 1/1,000), MX1 (PA5-22101, ThermoFisher Scientific; 1/1,000), MX2 (HPA030235, Sigma-Aldrich; 1/1,000), IFITM3 (11714-1-AP, ProteinTech; 1/1,000), and Actin (A1978, Sigma-Aldrich; 1/5,000), followed by secondary horseradish peroxidase-conjugated anti-mouse or anti-rabbit immunoglobulin antibodies and chemiluminescence (Bio-Rad). Images were acquired on a ChemiDoc[™] gel imaging system (Bio-Rad).

IAV production and infection

We have described previously IAV Nanoluciferase reporter virus generation (Doyle *et al*, 2018). Stocks were titrated by plaque assays on MDCK cells. IAV challenges were performed in serum-free DMEM for 1 h and the medium was subsequently replaced with DMEM containing 10%. IAV infection experiments were performed in triplicates in 96-well plates with cultures maintained for 16 h post-challenge. Nanoluciferase activity was measured with the Nano-Glo assay system (Promega), and luminescence was detected using a plate reader (Infinite[®] 200 PRO, Tecan).

VSV production and infection

A VSV-G pseudotyped-VSV-Δenv reporter virus, coding both GFP and Firefly Luciferase, was obtained from Gert Zimmer (Berger Rentsch & Zimmer, 2011). The virus was amplified on pMD.G transfected HEK293T and titrated thanks to the GFP reporter gene. For infection, 2.5 × 10⁴ cells per well in 96-well plates were infected at the indicated MOIs. 24 h after infection, cells were lysed and Firefly luciferase activity was measured (Firefly luciferase Assay System Promega).

Measles virus production and infection

Measles virus GFP strain (MV-GFP), which was kindly provided by F. Tangy (Institut Pasteur, Paris), was previously described (Combret *et al*, 2003). Viral stocks were produced on Vero cells. After 4 days of infection, supernatant was collected and then centrifuged to eliminate dead cells or fragments. Stocks were tittered using median tissue culture infectious dose assays (TCID₅₀) on Vero NK cells. Cells were infected with 10-fold serial dilutions of viral stocks and incubated for 7 days. Cells were then washed with PSB and fixed with 3% formaldehyde crystal violet during 30 min and finally rinsed with water. For infections, Huh-7 cells were infected at the indicated multiplicity of infection (MOI) in DMEM without FBS for

2 h in small volume of medium to enhance contacts with the inoculum and the cells. After 2 h, the viral inoculum was replaced with fresh DMEM 10% FBS 1% P/S. 24 h post-infection the cells were harvested and samples separated in half for Western blot and flow cytometry analysis.

CHIKV production and infection

The Nanoluciferase luciferase coding CHIKV construct was a gift from Andres Merits. The linearized plasmid coding CHIKV genome was transcribed with the mMACHINE mMACHINE SP6 kit (ThermoFischer Scientific) and 5×10^5 HEK293T were transfected with 1–4 μg of transcribed RNA, using Lipofectamine 2000 (ThermoFischer Scientific). After 24 h, supernatants were harvested, filtered and viruses were then amplified on baby hamster kidney (BHK21) cells. Stock titers were determined by plaque assays on Vero cells. For infections, 2.5×10^4 cells per well in 96-well plates were infected at the indicated MOIs. 24 h after infection, cells were lysed and Nanoluciferase activity was measured. WT CHIKV (98.2) has been described (Tsetsarkin *et al*, 2006). For the experiments using WT CHIKV, supernatants were harvested for plaque assay analysis and cells were lysed for RNA extraction 48 h post-infection. RT-qPCR analysis was then performed as described in the main methods, using primers 98.2-Forw 5'-ACGCAATTGAGCGAGGCAC-3', 98.2-Rev 5'-CGGAGGACATTGGGCCAC-3' and 98.2 probe 5'-FAM-CCCACACCGCATCGGCGTCGGCGAAGCTCC-TAMRA-3'. p98.2 was used to generate a standard curve and ensure the linearity of the assay (detection limit: at least 10 molecules per reaction).

SARS-CoV-2 production and infection

The SARS-CoV-2 BetaCoV/France/IDF0372/2020 isolate was supplied by Pr. Sylvie van der Werf and the National Reference Centre for Respiratory Viruses hosted by Institut Pasteur (Paris, France). The patient sample from which strain BetaCoV/France/IDF0372/2020 was isolated was provided by Dr. X. Lescure and Pr. Y. Yazdanpanah from the Bichat Hospital, Paris, France. The virus was amplified in Vero E6 cells (MOI 0.005) in serum-free media supplemented with 0.1 $\mu\text{g}/\text{ml}$ L-1-p-Tosylamino-2-phenylethyl chloromethylketone (TPCK)-treated trypsin (Sigma-Aldrich). The supernatant was harvested at 72 h post infection when cytopathic effects were observed (with around 50% cell death), cell debris were removed by centrifugation, and aliquots stored at -80°C . Viral supernatants were titrated by plaque assays in Vero E6 cells. Typical titers were 5.10^6 plaque forming units (PFU)/ml. Infections of A549-ACE2 cells were performed at the indicated multiplicity of infection (MOI; as calculated from titers obtained in Vero E6 cells) in serum-free DMEM and 5% serum-containing DMEM, respectively. The viral input was left for the duration of the experiment and cells lysed at 48 h post-infection for RT-qPCR analysis.

ZIKV NLuc reporter production and infection

The nanoluciferase expressing ZIKV construct has been described (Mutso *et al*, 2017). The corresponding linearized plasmid was transcribed *in vitro* using the mMACHINE mMACHINE™ SP6 transcription kit (ThermoFischer Scientific) and HEK293T cells were transfected with the transcribed RNA. After 7 days, supernatants

were harvested, filtered and stock titers were determined by plaque assays on Vero cells. For infections, 2.5×10^4 cells per well in 96-well plates were infected, at the indicated MOIs. 24 h after infection, cells were lysed and Nanoluciferase activity was measured using the Kit Nano Glo luciferase Assay (Promega).

YFV, DENV, ZIKV PF13, JEV flavivirus production and infection

YFV Asibi strain was provided by the Biological resource Center of Institut Pasteur. Stocks were produced on Vero NK cells. After 3 days of infection, viruses were concentrated by polyethylene glycol 6000 (PEG) precipitation and purified by centrifugation in a discontinuous gradient of sucrose. The Dengue 2 strain Malaysia SB8553 (DENV-2) was obtained from the Centro de Ingeniería Genética y Biotecnología (CIGB), Cuba. Stocks were generated on Vero NK cells. After 4 days of infection, viruses were concentrated by PEG 6000 precipitation. The Zika strain PF13 (kindly provided by V. M. Cao-Lormeau and D. Musso, Institut Louis Malardé, Tahiti Island, French Polynesia) was isolated from a viremic patient in French Polynesia in 2013. Stocks were produced on C6-36 cells. After 2 days of infection, viruses were concentrated by PEG 6000 precipitation and purified by centrifugation in a discontinuous gradient of sucrose. YFV Asibi and ZIKV titers were assessed by plaque assays using Vero NK cells, as described previously (Beauclair *et al*, 2020). DENV-2 was tittered by in cell western assays on Vero cells. Cells were fixed with PFA 4% during 30 min at room temperature (RT), then washed in PBS and permeabilized with 0.5% triton in PBS (Sigma-Aldrich) during 10 min at RT. Cells were then incubated 0.1% Tween in PBS (Sigma-Aldrich) containing 5% BSA (Sigma-Aldrich) during 1 h at RT prior to incubation with mouse anti-Env 4G2 antibodies overnight at 4°C . After 1 h of incubation with the secondary antibodies, cells were revealed with an Odyssey CLx infrared imaging system (Li-Cor Bioscience). Cells were infected at the indicated MOI in DMEM without FBS for 2 h in small volume of medium to enhance contacts with the inoculum and the cells. After 2 h, the viral inoculum was replaced with fresh DMEM 10% FBS 1% P/S. 24 h post-infection the cells were harvested and samples separated in half for Western blot and flow cytometry analysis. For the latter, cells were fixed and permeabilized using BD Cytofix/Cytoperm (Fisher scientific) for 30 min on ice (all the following steps were performed on ice and centrifuged at 4°C) and then washed three times with wash buffer. Cells infected with YFV, ZIKV and DENV-2 were incubated with the pan-flavivirus anti-Env 4G2 antibody for 1 h at 4°C and then with Alexa 488 anti-mouse IgG secondary antibodies (Thermo Fisher) for 45 min at 4°C in the dark. Data were acquired with an Attune NxT Acoustic Focusing Cytometer (Life technologies) and analyzed using FlowJo software.

HCoV-229E production and infection

HCoV-229E-Renilla was a gift from Volker Thiel (van den Worm *et al*, 2012) and was amplified for 5–7 days at 33°C in Huh7.5.1 cells (Zhong *et al*, 2005), in 5% FCS-containing DMEM. Virus stock concentration was assessed in Huh7.5.1 cells and titer was determined at 10^9 TCID50/ml. Cell were infected at the indicated TCID50s in DMEM 5% FCS at 33°C . 24 h later, cells were lysed and Renilla activity was measured using the Renilla Luciferase Assay System kit (Promega).

Recombinant DDX42 protein expression and purification

DDX42 coding sequence was subcloned from the aforementioned LV plasmid into pET-30 Ek/LIC expression vector (Novagen) using BamHI and XhoI cloning sites. The different inserts are in frame with the S- and His-tags and a sequence encoding the tobacco etch virus (TEV) protease cleavage site was inserted upstream of DDX42 coding region to enable tag removal during the protein purification process if needed. The recombinant plasmid pET30 ek/lic to express His-DDX42 was transformed in an *Escherichia coli* BL21 (DE3) strain resistant to Phage T1 (New England Biolabs) carrying pRARE2. One colony was used to inoculate an overnight culture of 125 ml LB medium supplemented with kanamycin (50 µg/ml) and chloramphenicol (34 µg/ml). This culture was diluted in 2.5 l of LB medium supplemented with the two antibiotics. Bacteria were grown at 16°C to an optical density at 600 nm of 0.8, then protein expression was induced with 1 mM Isopropyl-β-D-thiogalactoside (IPTG) and the culture was grown overnight at 16°C. Bacteria were harvested by centrifugation at 8,200 g for 20 min and resuspended in 30 ml buffer A (50 mM Tris-HCl pH 8, 400 mM NaCl, 5 mM MgCl₂, 7 mM β-mercaptoethanol, 40 mM imidazole, 10% glycerol and 1 mM benzamidine). Bacteria were disrupted by sonication and cell debris were removed by centrifugation at 28,000 g for 60 min. The supernatant was loaded at 4°C on Ni-NTA agarose beads previously equilibrated with buffer A. The beads were washed once with buffer A and twice with buffer B (50 mM Tris-HCl pH 8, 1 M NaCl, 5 mM MgCl₂, 7 mM β-mercaptoethanol, 40 mM imidazole and 10% glycerol) and elution was performed with buffer E (50 mM Tris-HCl pH 8, 200 mM NaCl, 5 mM MgCl₂, 7 mM β-mercaptoethanol, 500 mM imidazole, 10% glycerol). The eluted protein was then incubated in a dialysis-bag (cutoff 12–15 kDa) in 2 l dialysis buffer D (50 mM Tris-HCl pH 8, 200 mM NaCl, 5 mM MgCl₂, 5 mM β-mercaptoethanol) overnight at 4°C to remove imidazole, concentrated to 5 mg/ml using a Vivaspin column (50 kDa cutoff), loaded onto a size-exclusion chromatography column (Superdex 200 increase, GE Healthcare) and eluted with buffer F (50 mM Tris-HCl pH 8, 500 mM NaCl, 2 mM MgCl₂, 0.5 mM β-mercaptoethanol, 10% glycerol). Fractions B13, B14 and C1 (soluble proteins) from S200 chromatography were mixed together (Fig EV3B) and aliquots of purified His-tagged proteins were frozen in liquid nitrogen and stored at –80°C.

Poly(I:C) and G4 pull-downs

Biotinylated, high molecular weight poly(I:C) and 3'-Biotin-TEG labeled RNA oligonucleotides were ordered from InvivoGen and Eurofins, respectively; RNA oligonucleotide sequences were as follows: TRF2 G4 5'-CGGGAGGGCGGGGAGGGC-3' and Mutated (Mut.) TRF2 G4 5'-CGUGAGUGCGUGAGGGC-3' (Lavigne *et al*, 2021); and CHIKV G4 5'-GCAGGGCGUGCAAGGGGCGUGGAGCAGGGGAACGUGGUG. The latter is a sequence from CHIKV reference genome (GenBank accession number EU224268) predicted to potentially form G4s with G4Hunter algorithm (which allows to predict potential quadruplex forming sequences based on local guanine enrichment; Bedrat *et al*, 2016), using the MultiFastaSeeker Shiny application from (Lacroix, 2019). The 3'-Biotin-TEG labeled oligonucleotides were folded in 10 mM Tris-HCl pH 7.5, 100 mM KCl, 0.1 mM EDTA, with a 5 min 95°C denaturation followed by a slow cold down (2°C/min). High-affinity streptavidin magnetic beads

(Pierce, 88817) were equilibrated in blocking buffer (10 mM Tris-HCl pH 7.5, 100 mM KCl, 0.1 mM EDTA, 1 mM β-mercaptoethanol, RNase free BSA 0.1%) overnight. The beads were then incubated in blocking buffer with either the G4-folded oligonucleotides (5 pmol oligonucleotides/40 µl streptavidin magnetic beads) or with Poly(I:C) (0.1, 1 or 5 pmol/40 µl streptavidin magnetic beads) for 2 h at 4°C. After three washes with the washing buffer (10 mM Tris-HCl pH 7.5, 100 mM KCl, 0.1 mM EDTA, 1 mM β-mercaptoethanol), the beads were incubated in blocking buffer with 1 µg of recombinant proteins for 3 h at 4°C. Beads were then washed three times with washing buffer and retained proteins were finally eluted from the beads by a 5 min incubation at 95°C in 2X Laemmli buffer (100 mM Tris-HCl, pH 6.8, 4% SDS, 10% glycerol, 200 mM DTT, 0.1% bromophenol blue). Eluted proteins were analyzed by DDX42 immunoblotting. The input control represents 45 ng of DDX42 recombinant protein.

In vitro reverse transcription assays

Heat annealing of ODN

All annealing reactions were performed using 1 pmol of RNA 1–294 (corresponding to the first 294 nucleotides of HIV-1 NL4.3 RNA) and 0.3 pmol of [γ -³²P] 5'-end labeled ODN (5'-GTC CCT GTT CGG CCG CCA C-3', complementary to the Primer Binding Site of HIV-1 RNA). Primer and template were denatured 2 min at 90°C then cooled on ice. After addition of 50 mM Tris-HCl pH 8, 100 mM KCl, samples were incubated 20 min at 70°C, cooled on ice and supplemented with 5 mM MgCl₂ and 4 mM ATP. This corresponds to the primer/template complex (P/T).

Minus strand strong stop synthesis

To assay extension by HIV-1 RT, 30 nM of P/T complexes were incubated 4 min at 37°C with 85 nM HIV-1 RT in buffer RT (Tris-HCl pH 8 50 mM, KCl 40 mM, MgCl₂ 5 mM, DTT 1 mM), and reverse transcription was initiated by addition of dATP, dTTP, dGTP, and dCTP (100 µM each). After 1, 5, 20 and 60 min at 37°C, polymerase activity was stopped by adding 20 mM EDTA, and samples were treated with Proteinase K (1.9 µg/µl) during 30 min at 37°C. Samples were phenol/chloroform extracted and precipitated in ethanol 100%. Purified nucleic acids were resuspended in urea-containing loading buffer and analyzed by 8% PAGE. Radioactive bands were visualized and quantified using a BioImager BAS 2000 (Fuji). To test the influence of DDX42 on the elongation of reverse transcription, P/T complexes were incubated 4 min at 37°C with increasing concentrations of DDX42 (0.5, 1 or 2 µM). The reaction medium was then treated as described above.

Synthesis of +5 extension products with HIV-1 RT

The same experiment as in (Heat annealing of ODN) and (Minus strand strong stop synthesis) was performed (in presence or absence of increasing concentrations of DDX42), with the exception that extension was initiated by addition of dTTP, dGTP, dCTP (50 µM each) and 7.5 µM ddATP as a chain terminator.

Preparation of RNA-seq libraries

siRNA transfected U87-MG/CD4/CXCR4 and A549-ACE2 RNA extracts from three independent experiments were used for RNA-seq library preparation. After determining sample RNA integrity

numbers using a 2,100 Bioanalyzer (Agilent), ribosomal RNAs were depleted using the QIAseq FastSelect-rRNA HMR Kit (Qiagen) and libraries were prepared according to manufacturer's instructions using the QIAseq Stranded Total RNA Lib Kit (Qiagen). Libraries were quantified using a TapeStation D1000 ScreenTape. Equimolar amounts of each library were then mixed and sequenced on 2 lanes (2×150 bp) on the Illumina HiSeq 3000/4000 platform (GENEWIZ).

Analysis of high-throughput sequencing reads

Sequenced reads were filtered by quality and sequence adaptors removed using fastp v0.20.1 (<https://github.com/OpenGene/fastp>; Chen *et al*, 2018) with following parameters “fastp --qualified_quality_phred 20 --disable_length_filtering --detect_adapter_for_pe”. Reads were pseudo-mapped against human cDNA sequenced downloaded from Gencode database (<https://www.encodegenes.org/>) and transcripts abundance estimated with Kallisto v0.46.2 (<https://pachterlab.github.io/kallisto/about>; Bray *et al*, 2016) with parameters “--bias --bootstrap-samples 100”.

Differential analysis with DESeq2

Differential expressed genes upon siRNA transfection were obtained using DESeq2 (Love *et al*, 2014; version 1.32.0) in R (version 4.1.0). Briefly, transcript estimations were transformed in gene counts with tximport package (Soneson *et al*, 2015) and the differential expression obtained with the model design “~ condition + replicate”.

Pathway analysis

For each set of siRNA, a pathway analysis was performed using clusterProfiler R's package (Wu *et al*, 2021). Briefly, for each siRNA tested in each cell type, a pathways analysis was performed on differential upregulated or downregulated genes. Pathways enriched with an adj *P*-value < 0.05 were kept for the downstream analyses. For each selected pathways, the fold-change was calculated as the median fold-change of the DEGs involved in each pathway and displayed as a heatmap for comparison. All scripts are available in the GitLab deposit: <https://gitbio.ens-lyon.fr/LBMC/RMI2/siddx42-in-a549-and-u87-mg-cells>.

Statistical analyses

Statistical analyses were performed with GraphPad Prism. Analysis types are mentioned in figure legends and all comparisons are relative to the indicated controls. For data with experimental factors greater than two, multiple linear regression was performed. For data with two categorical factors, ANOVA was used, and repeated measures ANOVA when a pairing factor was present. Simple linear regression was used when the relationship between a continuous factor and a continuous response variable was investigated. *P* values are denoted as follow: ns, not significant, **P* < 0.05, ***P* < 0.01, ****P* < 0.001, *****P* < 0.0001.

Biosafety

Experiments with SARS-CoV-2, flaviviruses, chikungunya and lentiviruses were performed in BSL-3 laboratories, and experiments

with HCoV-229E, VSV, IAV, MV, and retroviral vectors in BSL-2 laboratories, following safety and security protocols approved by the risk prevention services of Institut Pasteur and CNRS.

Data availability

- 1 RNA-Seq data at Gene Expression Omnibus GSE207288: <https://www.ncbi.nlm.nih.gov/geo/query/acc.cgi?acc=GSE207288>.
- 2 The code used for RNA-seq analysis: <https://gitbio.ens-lyon.fr/LBMC/RMI2/siddx42-in-a549-and-u87-mg-cells>.

Expanded View for this article is available [online](#).

Acknowledgements

We wish to thank Zhanna Santybayeva ([illustration4science.com](https://www.illustration4science.com)) for the synopsis image, Tom Doyle and Chad Swanson for their useful comments on the manuscript, and Matthieu Lewis, Nadine Laguette, Nathalie Arhel, Juliette Fernandez, Jean-Luc Battini, Georg Kochs, Andres Merits, Frédéric Tangy, Daniela Verga, Sylvie van de Werf and Nathan Sherer for the generous provision of reagents, protocols and/or for helpful discussions. We are grateful to Guillaume Bec for the generous gift of HIV-1 RT and to Nicolas Manel and Helena Izquierdo-Fernandez for sharing their protocol for efficient knockdown in primary CD4⁺ T cell using CRISPR/Cas9 RNP electroporation. We are grateful to Myriam Boyer, Stéphanie Viala, Baptiste Monterroso and Orestis Faklaris from the imaging and flow cytometry facility MRI, for advice with flow cytometry and confocal microscopy, respectively. This work was supported by the Institut National de la Santé et de la Recherche Médicale (INSERM) (to CG), the ATIP-Avenir programme (to CG), institutional funds from the Centre National de la Recherche Scientifique (CNRS) and Montpellier University, Agence de Recherche ANRS France REcherche Nord&Sud Sida/HIV et Hépatites (ECTZ21792 to CG; ECTZ35478 to OM), Sidaction (to CG), a Starting Grant from the European Research Council (ERC StG 759226, ANTiViR) (to CG), PhD studentships from the Ministry of Higher Education and Research (to BB, JM and AR), and a 4th year PhD studentship from the Fondation pour la Recherche Médicale (to BB, FDT201904008024 and JM, FDT202106013175). SR and HP acknowledge financial support from the France Génomique National infrastructure, funded as part of “Investissement d'Avenir” program managed by Agence Nationale de la Recherche (ANR-10-INBS-09). We acknowledge the imaging facility MRI, member of the national infrastructure France-BioImaging supported by the French National Research Agency (ANR-10-INBS-04) and the BSL-3 facility CEMIPAI (UAR 3725 CNRS Montpellier University).

Author contributions

Boris Bonaventure: Data curation; formal analysis; validation; investigation; methodology; writing – original draft; writing – review and editing. **Antoine Rebendenne:** Formal analysis; validation; investigation; methodology. **Ana Luiza Chaves Valadão:** Formal analysis; investigation; methodology. **Mary Arnaud-Arnould:** Investigation; methodology; writing – review and editing. **Ségolène Gracias:** Investigation; methodology. **Francisco Garcia de Gracia:** Formal analysis; investigation. **Joe McKellar:** Investigation. **Emmanuel Labaronne:** Formal analysis. **Marine Tauziet:** Investigation. **Valérie Vivet-Boudou:** Formal analysis; investigation; methodology. **Eric Bernard:** Resources. **Laurence Briant:** Resources. **Nathalie Gros:** Investigation. **Wassila Djilli:** Investigation. **Valerie Courgnaud:** Resources. **Hugues Parrinello:** Investigation; methodology. **Stéphanie Rialle:** Software; formal analysis. **Mickaël Blaise:** Supervision; methodology; writing – review and editing. **Laurant Lacroix:** Resources; software. **Marc Lavigne:** Resources; supervision.

Jean-Christophe Paillart: Supervision; visualization; methodology. **Emiliano P Ricci:** Supervision; methodology. **Reiner Schulz:** Formal analysis. **Nolwenn Jouvenet:** Supervision; validation; visualization; methodology; writing – review and editing. **Olivier Moncorgé:** Conceptualization; formal analysis; supervision; writing – review and editing. **Caroline Goujon:** Conceptualization; resources; data curation; formal analysis; supervision; funding acquisition; validation; investigation; visualization; methodology; writing – original draft; project administration; writing – review and editing.

In addition to the CRediT author contributions, the contributions in detail are:

BB and CG designed the study, analyzed the data and wrote the manuscript with input from other authors. BB and CG performed the whole-genome screens and candidate validation. BB carried out most of the experiments, with assistance from AR, ALCV, FGdG, JM, MT, WD, AM, ALCV, MAA, OM and CG; VC provided some of the lentiviral vector stocks; EB and LB provided CHIKV stocks, NG performed ZIKV-Nluc infections, SG and NJ performed MeV, ZIKV PF13, DENV-2 and YFV infections; MAA produced recombinant DDX42 and did the pull-down assays with guidance from MB and ML; JCP and VV tested DDX42 activity *in vitro*; LL identified the predicted G4 in CHIKV genome; ML and ER analyzed the RNA-seq data; RS performed the statistical analyses; HP and SR performed the Illumina sequencing and MaGCK analyses, respectively. All authors have read and approved the manuscript.

Disclosure and competing interests statement

The authors declare that they have no conflict of interest.

References

- Adachi A, Gendelman HE, Koenig S, Folks T, Willey R, Rabson A, Martin MA (1986) Production of acquired immunodeficiency syndrome-associated retrovirus in human and nonhuman cells transfected with an infectious molecular clone. *J Virol* 59: 284–291
- Bainbridge JW, Stephens C, Parsley K, Demaison C, Halfyard A, Thrasher AJ, Ali RR (2001) *In vivo* gene transfer to the mouse eye using an HIV-based lentiviral vector; efficient long-term transduction of corneal endothelium and retinal pigment epithelium. *Gene Ther* 8: 1665–1668
- Beauclair G, Streicher F, Chazal M, Bruni D, Lesage S, Gracias S, Bourgeau S, Sinigaglia L, Fujita T, Meurs EF *et al* (2020) Retinoic acid inducible gene 1 and protein kinase R, but not stress granules, mediate the proinflammatory response to yellow fever virus. *J Virol* 94: e00403-20
- Bedrat A, Lacroix L, Mergny J-L (2016) Re-evaluation of G-quadruplex propensity with G4Hunter. *Nucleic Acids Res* 44: 1746–1759
- Berger Rentsch M, Zimmer G (2011) A vesicular stomatitis virus replicon-based bioassay for the rapid and sensitive determination of multi-species type I interferon. *PLoS One* 6: e25858
- Bonaventure B, Goujon C (2022) DEXH/D-box helicases at the frontline of intrinsic and innate immunity against viral infections. *J Gen Virol* 103 <https://doi.org/10.1099/jgv.0.001766>
- Bray NL, Pimentel H, Melsted P, Pachter L (2016) Near-optimal probabilistic RNA-seq quantification. *Nat Biotechnol* 34: 525–527
- Bulli L, Apolonia L, Kutzner J, Pollpeter D, Goujon C, Herold N, Schwarz S-M, Giernat Y, Keppler OT, Malim MH *et al* (2016) Complex interplay between HIV-1 capsid and MX2-independent IFN α -induced antiviral factors. *J Virol* 90: 7469–7480
- Burdick RC, Li C, Munshi M, Rawson JMO, Nagashima K, Hu W-S, Pathak VK (2020) HIV-1 uncoats in the nucleus near sites of integration. *Proc Natl Acad Sci U S A* 117: 5486–5493
- Cavrois M, de Noronha C, Greene WC (2002) A sensitive and specific enzyme-based assay detecting HIV-1 virion fusion in primary T lymphocytes. *Nat Biotechnol* 20: 1151–1154
- Chemudupati M, Kenney AD, Bonifati S, Zani A, McMichael TM, Wu L, Yount JS (2019) From APOBEC to ZAP: Diverse mechanisms used by cellular restriction factors to inhibit virus infections. *Biochim Biophys Acta Mol Cell Res* 1866: 382–394
- Chen S, Zhou Y, Chen Y, Gu J (2018) Fastp: An ultra-fast all-in-one FASTQ preprocessor. *Bioinformatics* 34: i884–i890
- Combredet C, Labrousse V, Mollet L, Lorin C, Delebecque F, Hurtrel B, McClure H, Feinberg MB, Brahic M, Tangy F (2003) A molecularly cloned Schwarz strain of measles virus vaccine induces strong immune responses in macaques and transgenic mice. *J Virol* 77: 11546–11554
- Corman VM, Landt O, Kaiser M, Molenkamp R, Meijer A, Chu DK, Bleicker T, Brünink S, Schneider J, Schmidt ML *et al* (2020) Detection of 2019 novel coronavirus (2019-nCoV) by real-time RT-PCR. *Euro Surveill* 25: 2000045
- Dharan A, Bachmann N, Talley S, Zwickelmaier V, Campbell EM (2020) Nuclear pore blockade reveals that HIV-1 completes reverse transcription and uncoating in the nucleus. *Nat Microbiol* 5: 1088–1095
- Doench JG (2018) Am I ready for CRISPR? a user's guide to genetic screens. *Nat Rev Genet* 19: 67–80
- Doyle T, Goujon C, Malim MH (2015) HIV-1 and interferons: who's interfering with whom? *Nat Rev Microbiol* 13: 403–413
- Doyle T, Moncorgé O, Bonaventure B, Pollpeter D, Lussignol M, Tauziet M, Apolonia L, Catanese M-T, Goujon C, Malim MH (2018) The interferon-inducible isoform of NCOA7 inhibits endosome-mediated viral entry. *Nat Microbiol* 3: 1369–1376
- Fan W, Mar KB, Sari L, Gaszek IK, Cheng Q, Evers BM, Shelton JM, Wight-Carter M, Siegwart DJ, Lin MM *et al* (2021) TRIM7 inhibits enterovirus replication and promotes emergence of a viral variant with increased pathogenicity. *Cell* 184: 3410–3425.e17
- Faulkner GJ, Billon V (2018) L1 retrotransposition in the soma: a field jumping ahead. *Mob DNA* 9: 22
- Fay MM, Lyons SM, Ivanov P (2017) RNA G-quadruplexes in biology: principles and molecular mechanisms. *J Mol Biol* 429: 2127–2147
- Gaddis NC, Sheehy AM, Ahmad KM, Swanson CM, Bishop KN, Beer BE, Marx PA, Gao F, Bibollet-Ruche F, Hahn BH *et al* (2004) Further investigation of simian immunodeficiency virus Vif function in human cells. *J Virol* 78: 12041–12046
- Ghimire D, Rai M, Gaur R (2018) Novel host restriction factors implicated in HIV-1 replication. *J Gen Virol* 99: 435–446
- Goodier JL, Cheung LE, Kazazian HH (2012) MOV10 RNA helicase is a potent inhibitor of Retrotransposition in cells. *PLoS Genet* 8: e1002941
- Goujon C, Malim MH (2010) Characterization of the alpha interferon-induced postentry block to HIV-1 infection in primary human macrophages and T cells. *J Virol* 84: 9254–9266
- Goujon C, Arfi V, Pertel T, Luban J, Lienard J, Rigal D, Darlix J-L, Cimarelli A (2008) Characterization of simian immunodeficiency virus SIVSM/human immunodeficiency virus type 2 Vpx function in human myeloid cells. *J Virol* 82: 12335–12345
- Goujon C, Moncorgé O, Bauby H, Doyle T, Ward CC, Schaller T, Hué S, Barclay WS, Schulz R, Malim MH (2013a) Human MX2 is an interferon-induced post-entry inhibitor of HIV-1 infection. *Nature* 502: 559–562
- Goujon C, Schaller T, Galão RP, Amie SM, Kim B, Olivieri K, Neil SJD, Malim MH (2013b) Evidence for IFN α -induced, SAMHD1-independent inhibitors of early HIV-1 infection. *Retrovirology* 10: 23
- Granneman S, Bernstein KA, Bleichert F, Baserga SJ (2006) Comprehensive mutational analysis of yeast DEXH/D box RNA helicases required for small ribosomal subunit synthesis. *Mol Cell Biol* 26: 1183–1194

- Haller O, Staeheli P, Schwemmler M, Kochs G (2015) Mx GTPases: dynamin-like antiviral machines of innate immunity. *Trends Microbiol* 23: 154–163
- Jimenez-Guardeño JM, Apolonia L, Betancor G, Malim MH (2019) Immunoproteasome activation enables human TRIM5 α restriction of HIV-1. *Nat Microbiol* 4: 933–940
- Kane M, Yadav SS, Bitzegeio J, Kutluay SB, Zang T, Wilson SJ, Schoggins JW, Rice CM, Yamashita M, Hatzioannou T et al (2013) MX2 is an interferon-induced inhibitor of HIV-1 infection. *Nature* 502: 563–566
- Kane M, Zang TM, Rihn SJ, Zhang F, Kueck T, Alim M, Schoggins J, Rice CM, Wilson SJ, Bieniasz PD (2016) Identification of interferon-stimulated genes with antiretroviral activity. *Cell Host Microbe* 20: 392–405
- Lacroix L (2019) G4HunterApps. *Bioinformatics* 35: 2311–2312
- Langmead B, Trapnell C, Pop M, Salzberg SL (2009) Ultrafast and memory-efficient alignment of short DNA sequences to the human genome. *Genome Biol* 10: R25
- Lavigne M, Helynck O, Rigoleto P, Boudria-Souilah R, Nowakowski M, Baron B, Brülé S, Hoos S, Raynal B, Guittat L et al (2021) SARS-CoV-2 Nsp3 unique domain SUD interacts with guanine quadruplexes and G4-ligands inhibit this interaction. *Nucleic Acids Res* 49: 7695–7712
- Lesage S, Chazal M, Beauclair G, Batalie D, Cerboni S, Couderc E, Lescure A, Del Nery E, Tangy F, Martin A et al (2022) Discovery of genes that modulate flavivirus replication in an interferon-dependent manner. *J Mol Biol* 434: 167277
- Li H, Handsaker B, Wysoker A, Fennell T, Ruan J, Homer N, Marth G, Abecasis G, Durbin R, 1000 Genome Project Data Processing Subgroup (2009) The sequence alignment/map format and SAMtools. *Bioinformatics* 25: 2078–2079
- Li W, Xu H, Xiao T, Cong L, Love MI, Zhang F, Irizarry RA, Liu JS, Brown M, Liu XS (2014) MAGeCK enables robust identification of essential genes from genome-scale CRISPR/Cas9 knockout screens. *Genome Biol* 15: 554
- Lin C-W, Cheng C-W, Yang T-C, Li S-W, Cheng M-H, Wan L, Lin Y-J, Lai C-H, Lin W-Y, Kao M-C (2008) Interferon antagonist function of Japanese encephalitis virus NS4A and its interaction with DEAD-box RNA helicase DDX42. *Virus Res* 137: 49–55
- Lindenmann J (1962) Resistance of mouse to mice adapted influenza A virus. *Virology* 16: 203–204
- Liu Z, Pan Q, Ding S, Qian J, Xu F, Zhou J, Cen S, Guo F, Liang C (2013) The interferon-inducible MxB protein inhibits HIV-1 infection. *Cell Host Microbe* 14: 398–410
- Liu N, Lee CH, Swigut T, Grow E, Gu B, Bassik MC, Wysocka J (2018) Selective silencing of euchromatic L1s revealed by genome-wide screens for L1 regulators. *Nature* 553: 228–232
- Love MI, Huber W, Anders S (2014) Moderated estimation of fold change and dispersion for RNA-seq data with DESeq2. *Genome Biol* 15: 550
- Mac Kain A, Maarifi G, Aicher S-M, Arhel N, Baidaliuk A, Munier S, Donati F, Vallet T, Tran QD, Hardy A et al (2022) Identification of DAXX as a restriction factor of SARS-CoV-2 through a CRISPR/Cas9 screen. *Nat Commun* 13: 2442
- Martin M (2011) Cutadapt removes adapter sequences from high-throughput sequencing reads. *EMBnetjournal* 17: 10–12
- Meertens L, Hafirassou ML, Couderc T, Bonnet-Madin L, Kril V, Kümmerer BM, Labeau A, Brugier A, Simon-Lorieri E, Burlaud-Gaillard J et al (2019) FHL1 is a major host factor for chikungunya virus infection. *Nature* 574: 259–263
- Miyashita M, Oshiumi H, Matsumoto M, Seya T (2011) DDX60, a DEXD/H box helicase, is a novel antiviral factor promoting RIG-I-like receptor-mediated signaling. *Mol Cell Biol* 31: 3802–3819
- Moncorge O, Long JS, Cauldwell AV, Zhou H, Lycett SJ, Barclay WS (2013) Investigation of influenza virus polymerase activity in pig cells. *J Virol* 87: 384–394
- Moran JV, Holmes SE, Naas TP, DeBerardinis RJ, Boeke JD, Kazazian HH (1996) High frequency retrotransposition in cultured mammalian cells. *Cell* 87: 917–927
- Moy RH, Cole BS, Yasunaga A, Gold B, Shankarling G, Varble A, Molleston JM, tenOever BR, Lynch KW, Cherry S (2014) Stem-loop recognition by DDX17 facilitates miRNA processing and antiviral defense. *Cell* 158: 764–777
- Mutso M, Saul S, Rausalu K, Susova O, Žusinaite E, Mahalingam S, Merits A (2017) Reverse genetic system, genetically stable reporter viruses and packaged subgenomic replicon based on a Brazilian zika virus isolate. *J Gen Virol* 98: 2712–2724
- Nakabayashi H, Taketa K, Miyano K, Yamane T, Sato J (1982) Growth of human hepatoma cells lines with differentiated functions in chemically defined medium. *Cancer Res* 42: 3858–3863
- Naldini L, Blömer U, Gallay P, Ory D, Mulligan R, Gage FH, Verma IM, Trono D (1996) *In vivo* gene delivery and stable transduction of nondividing cells by a lentiviral vector. *Science* 272: 263–267
- Ochsenauber C, Edmonds TG, Ding H, Keele BF, Decker J, Salazar MG, Salazar-Gonzalez JF, Shattock R, Haynes BF, Shaw GM et al (2012) Generation of transmitted/founder HIV-1 infectious molecular clones and characterization of their replication capacity in CD4 T lymphocytes and monocyte-derived macrophages. *J Virol* 86: 2715–2728
- OhAinle M, Helms L, Vermeire J, Roesch F, Humes D, Basom R, Delrow JJ, Overbaugh J, Emerman M (2018) A virus-packageable CRISPR screen identifies host factors mediating interferon inhibition of HIV. *Elife* 7: e39823
- O'Rourke JP, Newbound GC, Kohn DB, Olsen JC, Bunnell BA (2002) Comparison of gene transfer efficiencies and gene expression levels achieved with equine infectious anemia virus- and human immunodeficiency virus type 1-derived lentivirus vectors. *J Virol* 76: 1510–1515
- Oshiumi H, Miyashita M, Okamoto M, Morioka Y, Okabe M, Matsumoto M, Seya T (2015) DDX60 is involved in RIG-I-dependent and independent antiviral responses, and its function is attenuated by virus-induced EGFR activation. *Cell Rep* 11: 1193–1207
- Ostertag EM, Prak ET, DeBerardinis RJ, Moran JV, Kazazian HH (2000) Determination of L1 retrotransposition kinetics in cultured cells. *Nucleic Acids Res* 28: 1418–1423
- Parnas O, Jovanovic M, Eisenhaure TM, Herbst RH, Dixit A, Ye CJ, Przybylski D, Platt RJ, Tirosh I, Sanjana NE et al (2015) A genome-wide CRISPR screen in primary immune cells to dissect regulatory networks. *Cell* 162: 675–686
- Peng K, Muranyi W, Glass B, Laketa V, Yant SR, Tsai L, Cihlar T, Müller B, Kräusslich H-G (2014) Quantitative microscopy of functional HIV post-entry complexes reveals association of replication with the viral capsid. *Elife* 3: e04114
- Pennemann FL, Mussabekova A, Urban C, Stukalov A, Andersen LL, Grass V, Lavacca TM, Holze C, Oubraham L, Benamrouche Y et al (2021) Cross-species analysis of viral nucleic acid interacting proteins identifies TAOs as innate immune regulators. *Nat Commun* 12: 7009
- Rebendenne A, Valadão ALC, Tauziet M, Maarifi G, Bonaventure B, McKellar J, Planès R, Nisole S, Arnaud-Arnould M, Moncorge O et al (2021) SARS-CoV-2 triggers an MDA-5-dependent interferon response which is unable to control replication in lung epithelial cells. *J Virol* 95: e02415-20
- Rocak S (2005) Characterization of the ATPase and unwinding activities of the yeast DEAD-box protein Has1p and the analysis of the roles of the conserved motifs. *Nucleic Acids Res* 33: 999–1009

- Ruggiero E, Richter SN (2018) G-quadruplexes and G-quadruplex ligands: targets and tools in antiviral therapy. *Nucleic Acids Res* 46: 3270–3283
- Ryan-Graham MA, Peden KWC (1995) Both virus and host components are important for the manifestation of a Nef- phenotype in HIV-1 and HIV-2. *Virology* 213: 158–168
- Saenz DT, Teo W, Olsen JC, Poeschla EM (2005) Restriction of feline immunodeficiency virus by Ref1, Lv1, and primate TRIM5alpha proteins. *J Virol* 79: 15175–15188
- Sanjana NE, Shalem O, Zhang F (2014) Improved vectors and genome-wide libraries for CRISPR screening. *Nat Methods* 11: 783–784
- Schaller T, Ocwieja KE, Rasaiyaah J, Price AJ, Brady TL, Roth SL, Hué S, Fletcher AJ, Lee K, KewalRamani VN et al (2011) HIV-1 capsid-cyclophilin interactions determine nuclear import pathway, integration targeting and replication efficiency. *PLoS Pathog* 7: e1002439
- Schindelin J, Arganda-Carreras I, Frise E, Kaynig V, Longair M, Pietzsch T, Preibisch S, Rueden C, Saalfeld S, Schmid B et al (2012) Fiji: an open-source platform for biological-image analysis. *Nat Methods* 9: 676–682
- Schoggins JW (2019) Interferon-stimulated genes: what do they all do? *Annu Rev Virol* 6: 567–584
- Schoggins JW, Wilson SJ, Panis M, Murphy MY, Jones CT, Bieniasz P, Rice CM (2011) A diverse range of gene products are effectors of the type I interferon antiviral response. *Nature* 472: 481–485
- Shalem O, Sanjana NE, Hartenian E, Shi X, Scott DA, Mikkelsen TS, Heckl D, Ebert BL, Root DE, Doench JG et al (2014) Genome-scale CRISPR-Cas9 knockout screening in human cells. *Science* 343: 84–87
- Shalem O, Sanjana NE, Zhang F (2015) High-throughput functional genomics using CRISPR-Cas9. *Nat Rev Genet* 16: 299–311
- Simon JH, Southerling TE, Peterson JC, Meyer BE, Malim MH (1995) Complementation of vif-defective human immunodeficiency virus type 1 by primate, but not nonprimate, lentivirus vif genes. *J Virol* 69: 4166–4172
- Soneson C, Love MI, Robinson MD (2015) Differential analyses for RNA-seq: transcript-level estimates improve gene-level inferences. *F1000Research* 4: 1521
- Taschuk F, Cherry S (2020) DEAD-box helicases: sensors, regulators, and effectors for antiviral defense. *Viruses* 12: 181
- Taschuk F, Tapescu I, Moy RH, Cherry S (2020) DDX56 binds to chikungunya virus RNA to control infection. *MBio* 11: e02623-20
- Tenthorey JL, Emerman M, Malik HS (2022) Evolutionary landscapes of host-virus arms races. *Annu Rev Immunol* 40: 271–294
- Tsetsarkin K, Higgs S, McGee CE, Lamballerie XD, Charrel RN, Vanlandingham DL (2006) Infectious clones of chikungunya virus (La Réunion isolate) for vector competence studies. *Vector Borne Zoonotic Dis* 6: 325–337
- Uhlmann-Schiffler H, Jalal C, Stahl H (2006) Ddx42p--a human DEAD box protein with RNA chaperone activities. *Nucleic Acids Res* 34: 10–22
- Uhlmann-Schiffler H, Kiermayer S, Stahl H (2009) The DEAD box protein Ddx42p modulates the function of ASPP2, a stimulator of apoptosis. *Oncogene* 28: 2065–2073
- Wei J, Alfajaro MM, DeWeirdt PC, Hanna RE, Lu-Culligan WJ, Cai WL, Strine MS, Zhang S-M, Graziano VR, Schmitz CO et al (2020) Genome-wide CRISPR screens reveal host factors critical for SARS-CoV-2 infection. *Cell* 184: 76–91.e13
- Will CL, Urlaub H, Achsel T, Gentzel M, Wilm M, Lührmann R (2002) Characterization of novel SF3b and 17S U2 snRNP proteins, including a human Prp5p homologue and an SF3b DEAD-box protein. *EMBO J* 21: 4978–4988
- Wingett SW, Andrews S (2018) FastQ Screen: a tool for multi-genome mapping and quality control. *F1000Research* 7: 1338
- van den Worm SHE, Eriksson KK, Zevenhoven JC, Weber F, Züst R, Kuri T, Dijkman R, Chang G, Siddell SG, Snijder EJ et al (2012) Reverse genetics of SARS-related coronavirus using vaccinia virus-based recombination. *PLoS One* 7: e32857
- Wu T, Hu E, Xu S, Chen M, Guo P, Dai Z, Feng T, Zhou L, Tang W, Zhan L et al (2021) clusterProfiler 4.0: a universal enrichment tool for interpreting omics data. *Innovations* 2: 100141
- Xu B, Pan Q, Liang C (2018) Role of MxB in alpha interferon-mediated inhibition of HIV-1 infection. *J Virol* 92: e00422-18
- Zhong J, Gastaminza P, Cheng G, Kapadia S, Kato T, Burton DR, Wieland SF, Uprichard SL, Wakita T, Chisari FV (2005) Robust hepatitis C virus infection *in vitro*. *Proc Natl Acad Sci U S A* 102: 9294–9299
- Zhou A (1993) Expression cloning of 2-5A-dependent RNAase: A uniquely regulated mediator of interferon action. *Cell* 72: 753–765
- Zilberstein A, Kimchi A, Schmidt A, Revel M (1978) Isolation of two interferon-induced translational inhibitors: A protein kinase and an oligoadenylate synthetase. *Proc Natl Acad Sci U S A* 75: 4734–4738
- Zürcher T, de la Luna S, Sanz-Ezquerro JJ, Nieto A & Ortín J (1996) Mutational analysis of the influenza virus a/Victoria/3/75 PA protein: Studies of interaction with PB1 protein and identification of a dominant negative mutant. *J Gen Virol* 77(Pt 8): 1745–1749
- Zyner KG, Mulhearn DS, Adhikari S, Martínez Cuesta S, Di Antonio M, Erard N, Hannon GJ, Tannahill D, Balasubramanian S (2019) Genetic interactions of G-quadruplexes in humans. *Elife* 8: e46793



License: This is an open access article under the terms of the [Creative Commons Attribution-NonCommercial-NoDerivs](https://creativecommons.org/licenses/by-nc-nd/4.0/) License, which permits use and distribution in any medium, provided the original work is properly cited, the use is non-commercial and no modifications or adaptations are made.

Expanded View Figures

Figure EV1. IFN induces a strong inhibition of HIV-1 in T98G cells, which is lost in cells enriched in the CRISPR screen.

- A T98G/Cas9/CD4/CXCR4/Firefly cells were pre-treated with IFN for 24 h prior to infection with increasing doses of NL4-3 Renilla (NL4-3/Nef-IRES-Renilla) (indicated in ng p24^{Gag}). Renilla activity was normalized to Firefly activity and the relative infection efficiencies are shown. Data represent the average and standard deviation (s.d.) of 3 biological replicates.
- B GeCKO control cells and enriched cells from 3 successive rounds of selection (Round 1, 2, and 3, as indicated) were treated with IFN or not and infected with GFP-expressing lentiviral vectors. The percentage of infected cells was evaluated by flow cytometry 2 days post-infection. Data represent the average of 2 biological replicates.
- C The indicated primary cells or immortalized cell cultures were treated with IFN for 24 h or left untreated. RNA was subsequently extracted and DDX42 and ISG15 (a prototype ISG) mRNA levels were quantified by RT-qPCR; ActinB and GAPDH were used as endogenous controls. The bar chart shows the relative levels of expression of DDX42 and ISG15 in the presence or absence of IFN treatment. Data represent the mean \pm S.E.M of 3 biological replicates.

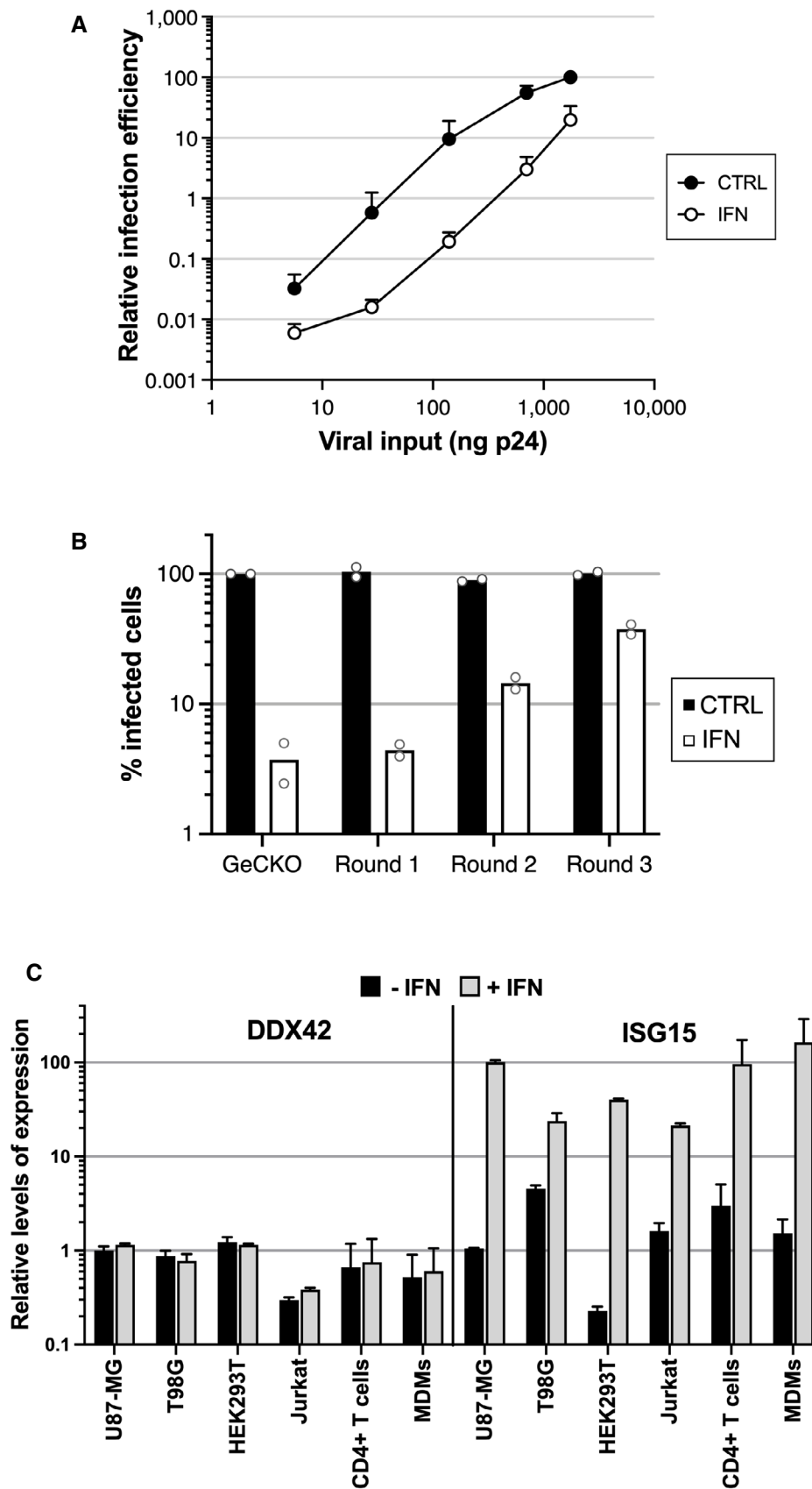


Figure EV1.

Figure EV2. DDX42 inhibits HIV-1 infection independently of the IFN response.

- A Cell viability of siRNA-transfected U87-MG/CD4/CXCR4 cells was assessed 72 h post-transfection by measuring ATP levels. Data represent the mean \pm S.E.M of 3 biological replicates.
- B U87-MG/CD4/CXCR4 cells were transfected with siRNAs, pre-treated or not with IFN and infected with WT HIV-1 (NL4-3) in the presence or not of reverse transcription inhibitors (AZT/3TC). 48 h later, cells were lysed, RNA extracted and RT-qPCR analysis performed to measure HIV-1 RNAs. Data represent the mean \pm S.E.M of 4 biological replicates. Two-way ANOVA on log-transformed data with Sidak's test.
- C Supernatants from (B) were harvested 48 h post-infection and AlphaLisa used to measure CA p24^{Gag} production. Data represent the mean \pm S.E.M of 4 biological replicates. Two-tailed, unpaired *t* test.
- D RT-qPCR analysis was performed RNA samples from (B) to measure relative expression of the ISG OAS1, ISG15, and MX1 (normalized to actin and GAPDH). Data represent the mean \pm S.E.M of 4 biological replicates. Two-way ANOVA with Dunnett's test.
- E U87-MG/CD4/CXCR4 cells were transduced to express Cas9 and sgRNAs either targeting nothing (CTRL) or IRF9 and STAT1 (IRF9/STAT1). After 2 weeks, cells were treated or not with IFN, and, 48 h later, IFITM3 and MX2 induction was analyzed by immunoblotting, Actin served as a loading control. A representative immunoblot is shown.
- F siRNA-transfected MDMs were harvested 48 h post-transfection for RNA extraction and quantification of DDX42 mRNA levels by RT-qPCR. Actin and GAPDH were used as endogenous controls. Data represent the mean \pm S.E.M of 3 biological replicates performed with cells from different blood donors (parallel samples from Fig 2E). One-way ANOVA with Dunnett's test.
- G U87-MG/CD4/CXCR4 cells were transduced with lentiviral vectors expressing either Firefly (negative control), WT DDX42 (WT) or a motif I point mutant, which has an impaired ATPase activity (K303E). Transduced cells were infected with HIV-1 Renilla (NL4-3/Nef-IRES-Renilla) and the infection efficiency was assessed 24 h later by measuring Renilla activity. Data represent the mean \pm S.E.M of 3 biological replicates. Two-way ANOVA on log-transformed data with Dunnett's test.

Data information: *P* values are denoted as follow: ns, not significant, **P* < 0.05, ***P* < 0.01, ****P* < 0.001.

Source data are available online for this figure.

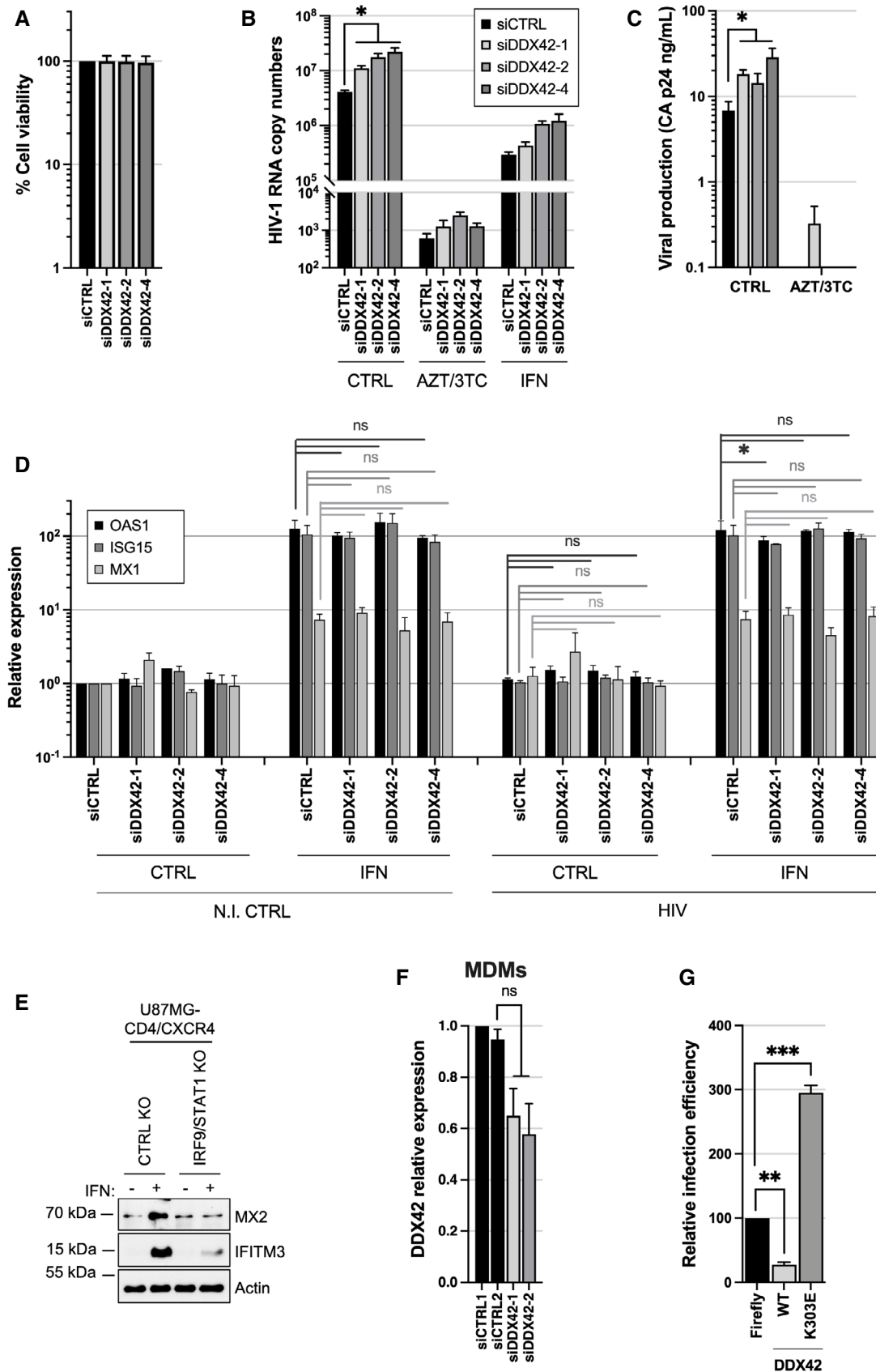


Figure EV2.

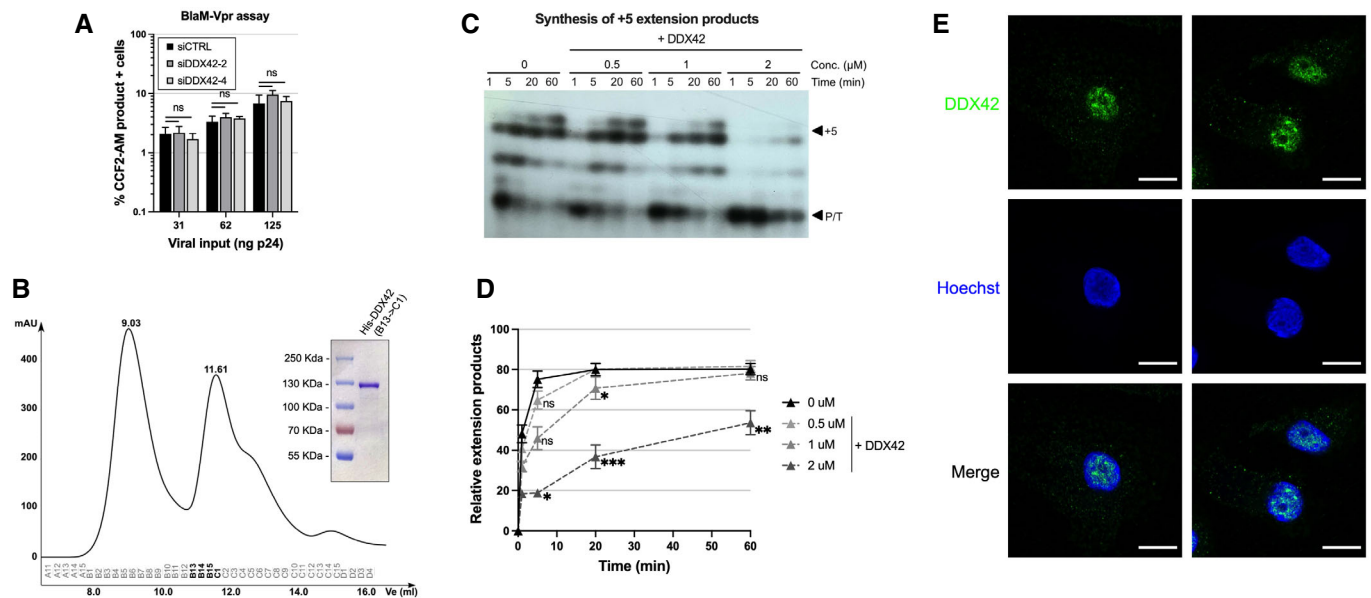


Figure EV3. DDX42 does not impact HIV-1 entry and impairs reverse transcription *in vitro*.

- A DDX42-depleted U87-MG/CD4/CXCR4 cells were infected with the indicated amounts of NL4-3/Nef-IRES-Renilla viruses carrying the β -lactamase (BlaM)-Vpr fusion protein for 3 h. The cells were subsequently loaded with CCF2-AM substrate dye for 2 h, washed extensively and incubated for another 16 h for the reaction to develop. Cells positive for the CCF2-AM product were scored by flow cytometry. Data represent the mean \pm S.E.M of 3 biological replicates. Two-way ANOVA on log-transformed data with Dunnett's test. *P* values are denoted as follow: ns, not significant, **P* < 0.05, ***P* < 0.01, ****P* < 0.001, *****P* < 0.0001.
- B Elution profile of His-DDX42. Top right, SDS-PAGE followed by Coomassie coloration analysis of the pooled fractions.
- C Heat-annealed ODN/RNA 1–294 complex was incubated with HIV-1 RT and the indicated, increasing concentrations of recombinant DDX42 (Fig EV3B). Reverse transcription was initiated by addition of dTTP, dGTP, dCTP and ddATP. Extension was for 1, 5, 20 or 60 min and samples were analyzed by PAGE 12% (P/T: primer/template; +5: extension of 5 nucleotides). A representative autoradiograph is shown.
- D Quantified data correspond to the ratio of extension products / unextended P/T at different time points. Data represent the mean \pm S.E.M of 4 biological replicates. Two-way ANOVA on log-transformed data with Dunnett's test. *P* values are denoted as follow: ns, not significant, **P* < 0.05, ***P* < 0.01, ****P* < 0.001.
- E MDMs were fixed, endogenous DDX42 and the nuclei were visualized using DDX42-specific antibodies and Hoechst staining, respectively, and confocal microscopy. Representative images are shown. Scale bar, 10 μ m.

Figure EV4. DDX42 antiviral activity and impact on ISG induction.

- A DDX42 silencing efficiency in U87-MG, A549-ACE2, Huh-7 and Huh-7.5.1 cells.
- B Relative ZIKV PF13 infection efficiency in siRNA-transfected Huh-7 cells analyzed by flow cytometry. Two-way ANOVA with Sidak's test on log-transformed data.
- C ZIKV PF13 infection efficiency in control (CTRL) and IFN-treated, siRNA-transfected U87-MG cells analyzed by RT-qPCR and expressed as genome equivalents (GE) per μ g of total cellular RNA. Two-way ANOVA with Sidak's test on log-transformed data.
- D JEV infection efficiency in control (CTRL) and IFN-treated, siRNA-transfected U87-MG cells analyzed by RT-qPCR by RT-qPCR and expressed as genome equivalents (GE) per μ g of total cellular RNA. Two-way ANOVA with Sidak's test on log-transformed data.
- E Relative expression of the ISGs OAS1, ISG15, and MX1 (normalized to actin and GAPDH) measured by RT-qPCR in parallel samples from (C) and (D). Two-way ANOVA with Dunnett's test.
- F Relative YFV infection efficiency in siRNA-transfected Huh-7 cells analyzed by flow cytometry. Two-way ANOVA with Sidak's test on log-transformed data.
- G Relative DENV-2 infection efficiency in siRNA-transfected Huh-7 cells analyzed by flow cytometry. Two-way ANOVA with Sidak's test on log-transformed data.
- H Relative expression of the ISGs OAS1, ISG15, and MX1 (normalized to actin and GAPDH) measured by RT-qPCR in parallel samples from Fig 4F. Two-way ANOVA with Dunnett's test.
- I CTRL and IRF9/STAT1 KO A549-ACE2 cells were pre-treated or not with IFN for 24 h and lysed for immunoblot analysis to measure MX1 and IFITM3 induction, Actin served as a loading control. A representative immunoblot is shown.

Data information: (A–H). Mean \pm SEM of 3 biological replicates (4 for the silencing efficiency in A549-ACE2 cells). *P* values are denoted as follow: ns, not significant, **P* < 0.05, ***P* < 0.01, ****P* < 0.001, *****P* < 0.0001.

Source data are available online for this figure.

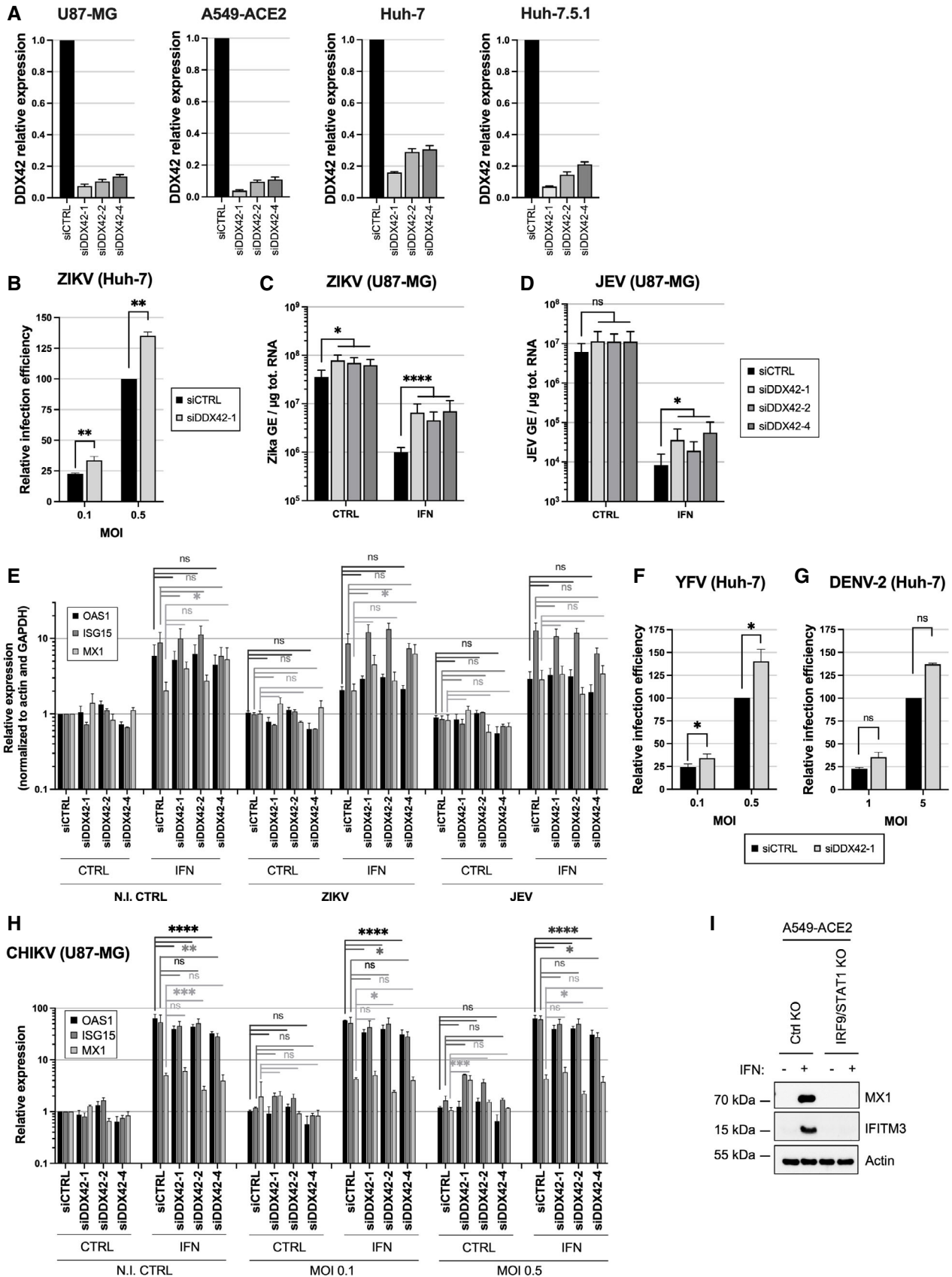


Figure EV4.

Figure EV5. Impact of DDX42 silencing on the cellular transcriptome.

- A Venn diagram showing the Differentially Expressed Genes (DEGs) overlap between siRNA conditions in U87-MG cells, A549 cells and DEGs overlapping between U87-MG and A549 cells using cutoff criteria of \log_2 fold change (\log_2FC) > 1 and P value < 0.05 .
- B, C Comparison of the effects of the different siRNAs tested in U87-MG (B) and A549-ACE2 (C) cells. For each cell type, pairwise fold-change comparison of the effect of each siRNA are showed on the scatter plots on the left side. The heatmaps show the median fold-change of the DEG involved in each pathway for each siRNA tested (right side). Gray boxes refer to non-significantly enriched pathways.

Refer to Dataset [EV1](#) for the identity of the DEGs.

